Development of a new microdosimetric biological weighting function for the RBE10 assessment in case of the V79 cell line exposed to ions from 1H to 238U

Peer-reviewed author version

Parisi, Alessio; Sato, Tatsuhiko; Matsuya, Yusuke; Kase, Yuki; Magrin, Giulio; Verona, Claudio; Tran , Linh T; Rosenfeld, Anatoly B; BIANCHI, Anna; Olko, Pawel; Struelens, Lara & Vanhavere, Filip (2020) Development of a new microdosimetric biological weighting function for the RBE10 assessment in case of the V79 cell line exposed to ions from 1H to 238U. In: Physics in medicine and biology (Print),65(23) (Art N° 235010).

DOI: 10.1088/1361-6560/abbf96
Handle: http://hdl.handle.net/1942/32538

Physics in Medicine & Biology

Development of a new microdosimetric biological weighting function for the RBE_{10} assessment in case of the V79 cell line exposed to ions from ^{1}H to ^{238}U

To cite this article before publication: Alessio Parisi *et al* 2020 *Phys. Med. Biol.* in press https://doi.org/10.1088/1361-6560/abbf96

Development of a new microdosimetric biological weighting function for the RBE_{10} assessment in case of the V79 cell line exposed to ions from ^{1}H to ^{238}U

Alessio Parisi [a, *], Tatsuhiko Sato [b], Yusuke Matsuya [b], Yuki Kase [c], Giulio Magrin [d], Claudio Verona [e], Linh Tran [f], Anatoly Rosenfeld [f], Anna Bianchi [a], Pawel Olko [g], Lara Struelens [a], Filip Vanhavere [a]

[a] Belgian Nuclear Research Centre (SCK CEN), Mol, Belgium

[b] Japan Atomic Energy Agency (JAEA), Tokai-Mura, Japan

[c] Radiation and Proton Therapy Center, Shizuoka Cancer Center (SCC), Shizuoka, Japan

[d] MedAustron Ion Therapy Center, Wiener Neustadt, Austria

[e] Industrial Engineering Department, University of Rome "Tor Vergata", Rome, Italy

[f] Centre for Medical Radiation Physics (CMRP), University of Wollongong, Wollongong, Australia

[h] Institute of Nuclear Physics, Polish Academy of Sciences (IFJ PAN), Krakow, Poland

* corresponding author, email address: alessio.parisi@sckcen.be

Keywords: biophysical modeling, relative biological effectiveness, microdosimetry, radiobiological weighting function, microdosimetric kinetic model, PHITS

Abbreviations used in the article

BWF = biological weighting function (Loncol et al., 1994)

CAL = Centre Antoine Lacassagne (Nice, France)

CATANA = Center for Hadron Therapy and Advanced Nuclear Applications (Catania, Italy)

CCB = Centrum Cyklotronowe Bronowice at the Institute of Nuclear Physics (Krakow, Poland)

CNAO = National Center for Oncological Hadron Therapy (Pavia, Italy)

DNA = deoxyribonucleic acid

GSI = Centre for Heavy Ion Research (Darmstadt, Germany)

HIAF = Heavy Ion Accelerator Facility at the Australian National University (Canberra, Australia)

HIMAC = Heavy Ion Medical Accelerator in Chiba (Chiba, Japan)

IBWF = improved biological weighting function (this work)

LDPE = low density polyethylene

LET = linear energy transfer

MGH = Massachusetts General Hospital (Boston, United States of America)

modified MKM = modified microdosimetric kinetic model (Kase et al., 2006)

OCL = Oslo Cyclotron Laboratory (Oslo, Norway)

PHITS = Particle and Heavy Ion Transport code System (Sato et al., 2018)

PIDE = Particle Irradiation Data Ensemble (Friedrich et al., 2013)

PMMA = poly(methyl methacrylate)

PMRC = Proton Medical Research Center (Tsukuba, Japan)

RBE = relative biological effectiveness

S = surviving fraction

SOBP = spread out Bragg peak

SRIM = Stopping and Range of Ions in Matter (Ziegler et al., 2010)

TEPC = tissue equivalent proportional counter

V79 cell line = Chinese hamster lung fibroblast

Abstract

An improved biological weighting function (IBWF) is proposed to phenomenologically relate microdosimetric lineal energy probability density distributions with the relative biological effectiveness (RBE) for the *in vitro* clonogenic cell survival (surviving fraction = 10%) of the most commonly used mammalian cell line, i.e. the Chinese hamster lung fibroblasts (V79). The IBWF, intended as a simple and robust tool for a fast RBE assessment to compare different exposure conditions in particle therapy beams, was determined through an iterative global-fitting process aimed to minimize the average relative deviation between RBE calculations and literature *in vitro* data in case of exposure to various types of ions from ^{1}H to ^{238}U. By using a single particle- and energy- independent function, it was possible to establish an univocal correlation between lineal energy and clonogenic cell survival for particles spanning over an unrestricted linear energy transfer (LET) range of almost five orders of magnitude (0.2 to 15000 keV/μm in liquid water). The average deviation between IBWF-derived RBE values and the published *in vitro* data was ~14%.

The IBWF results were also compared with corresponding calculations (*in vitro* RBE_{10} for the V79 cell line) performed using the modified microdosimetric kinetic model (modified MKM). Furthermore, RBE values computed with the reference biological weighting function (BWF) for the *in vivo* early intestine tolerance in mice were included for comparison and to further explore potential correlations between the BWF results and the *in vitro* RBE as reported in previous studies. The results suggest that the modified MKM possess limitations in reproducing the experimental *in vitro* RBE_{10} for the V79 cell line in case of ions heavier than ^{20}Ne. Furthermore, due to the different modelled endpoint, marked deviations were found between the RBE values assessed using the reference BWF and the IBWF for ions heavier than ^{2}H.

Finally, the IBWF was unchangingly applied to calculate RBE values by processing lineal energy density distributions experimentally measured with 8 different microdosimeters in 19 ^{1}H and ^{12}C beams at 10 different facilities (8 clinical and 2 research ones). Despite the differences between the detectors, irradiation facilities, beam profiles (pristine or spread out Bragg peak), maximum beam energy, beam delivery (passive or active scanning), energy degradation system (water, PMMA, polyamide or low density polyethylene), the obtained

IBWF-based RBE trends were found to be in good agreement with the corresponding ones in case of computer-simulated microdosimetric spectra (average relative deviation equal to 0.8% and 5.7% for ^{1}H and ^{12}C ions respectively).

1. Introduction

Radiation effects on living entities are strongly related to the microscopic pattern of energy deposition at cellular and subcellular scale (Scholz, 2003), with the differences in the clustering of damages to the of deoxyribonucleic acid (DNA) damages (i.e. single and double strand breaks) currently considered as the main cause for initiating the processes which will finally determine the consequences of the exposure to different radiation qualities (McMahon and Prise, 2019). With the increasing use of charged particles for cancer radiotherapy (Durante and Paganetti, 2016), it appears of primary importance to quantify and model these effects for treatment planning, quality control and research purposes. While in case of proton radiotherapy the relative biological effectiveness (RBE) may be linearly-correlated with the unrestricted proton dose-mean linear energy transfer (LET) (Paganetti, 2014), for heavier particles more refined approaches are needed to account for the overkill effect and not-unique LET dependence of the RBE for different particles (Friedrich et al., 2013). Furthermore, in a similar way the specific radiosensitivity of the cell line and the biological endpoint should be considered in the calculations as well as the exposure conditions as the dose, the dose rate and the oxygen level.

To this regard, many biophysical models such as the Gamma-kill and Ion-kill Cell Inactivation Theory (Katz et al., 1971), the Theory of Dual Radiation Action (TDRA, Kellerer and Rossi, 1974, Kellerer and Rossi, 1978), the Microdosimetric Kinetic Model (MKM, Hawkins, 1994, Hawkins, 2003), Biological Weighting Functions (BWFs, Loncol et al., 1994, Pihet and Menzel, 1999), the Local Effect Model (LEM, Scholz et al., 1997, Elsässer and Scholz, 2007, Elsässer et al., 2010), the RBE matrix (Wroe et al., 2009), the modified Microdosimetric Kinetic Model (modified MKM, Kase et al., 2006), the Repair-Misrepair-Fixation model (RMF, Carlson et al., 2008, Frese et al., 2012, Guan et al., 2018), the Stochastic and Double-Stochastic Microdosimetric Kinetic

Models (SMKM and DSMKM, Sato and Furusawa, 2012, Sato and Hamada, 2014, Inaniwa and Kanematsu, 2018), the Giant Loop Binary Lesion model (GLOBE, Friedrich et al., 2012, Friedrich et al., 2014), the Biophysical Analysis of Cell Death and Chromosome Aberrations model (BIANCA, Ballarini et al., 2013, Carante et al., 2018), the Nanodosimetry and Oxidative Stress model (NanOx, Cunha et al., 2017, Monini et al., 2018), mechanistic models (McMahon et al., 2016, McMahon et al., 2017) and the Integrated Microdosimetric Kinetic Model (IMKM, Matsuya et al., 2018) were proposed to relate physical quantities (i.e. lineal energy or radial dose distribution) with biological endpoints such as DNA damage, chromosome aberration and cell survival. Considering tumor control probability, clonogenic cell survival is considered as the most clinically relevant endpoint and consequently it is the most frequently studied worldwide (Paganetti et al., 2019). Among all proposed models, those based on microdosimetry possess the advantage to deal with physical quantities such as the specific energy and the lineal energy whose probability density distributions are experimentally measurable (International Commission on Radiation Units and Measurements, 1983).

The two most-commonly used microdosimetric approaches are the modified microdosimetric kinetic model (modified MKM, Kase et al., 2006, biological endpoint = *in vitro* cell survival) and the biological weighting function (BWF, Loncol et al., 1994, biological endpoint = *in vivo* early intestine tolerance). In the first case, although deviations between the modified MKM results and experimental *in vitro* data were preliminary observed and discussed for ^{56}Fe ions with LET in water greater than 450 keV/μm (Kase et al., 2006), a detailed investigation of its performances for modeling the cell survival over a broad particle and energy range is still missing. Secondly, although a good correlation was found between the BWF results and the *in vitro* RBE for human tongue cell carcinoma (De Nardo et al., 2004 b), human melanoma cells (De Nardo et al., 2004 b), asynchronous Chinese hamster lung fibroblast V79 cells (Conte et al., 2019) and human glioblastoma U87 cells (Colautti et al., 2020) in case of proton exposures, for ^{12}C ions a relevant RBE underestimation was reported in respect to simulations with the local effect model (LEM, Gerlach et al., 2002) and the correlation between the two data series (BWF results and *in vitro* RBE) was not further explored.

Thus, in this article the accuracy of the RBE_{10} calculations performed with modified MKM in case of the V79 cell line was systematically benchmarked through a comparison against published *in vitro* cell survival data for ions up to ^{238}U. The latter cell line was chosen because is the most frequently used and the most abundant in literature. Furthermore, it was investigated if the correlation between the BWF results and the *in vitro* RBE observed in case of proton exposures might hold also for heavier ions. Due to shortcomings in the obtained results, an upgraded approach making use of an improved biological weighting function (IBWF) is proposed to establish a phenomenological correlation between microdosimetric lineal energy spectra and the RBE_{10} in case of V79 cells exposed to ions ranging from ^{1}H and ^{238}U. The latter function was determined through an iterative process between computer simulated microdosimetric spectra in water and the published *in vitro* data. Finally, in order to preliminarily investigate the applicability of the IBWF to experimentally-measured microdosimetric lineal energy distributions, the IBWF was used in combination with microdosimetric spectra acquired with 8 different gas- and solid- state detectors in different ^{1}H and ^{12}C beams. The RBE-vs-$\bar{y}_D$ trends, obtained for the different microdosimeter-exposure combinations, were compared to each other and benchmarked against the corresponding results of the aforementioned computer simulations.

2. Methodology

2.1. Computer simulations

All radiation transport simulations included in this work were performed using the Monte Carlo Particle and Heavy Ion Transport code System (PHITS) version 3.09 (Sato et al., 2018). The frequency- and dose- probability density of the lineal energy needed for the RBE calculations were assessed employing the microdosimetric analytical function (Sato et al., 2006) implemented in the PHITS [T-SED] tally. The analytical function was developed to reproduce the results of simulations performed using the track structure code TRACEL (Tomita et al., 1997) and validated against experimental data gathered with gas-based detectors in case of exposures to a wide range of ions (Schmollack et al., 2000, Tsuda et al., 2012), neutrons (Hu et al., 2020) and within clinical proton beams (Takada et al., 2017). More details on the development of the PHITS microdosimetric function can be found in Sato et al., 2006 and Sato et al., 2012.

Monoenergetic beams (simulated energies = 0.1, 0.2, 0.3. 0.4, 0.5, 0.6, 0.7, 0.8, 0.9, 1, 2, 3, 4, 5, 6, 7, 8, 9, 10, 20, 30, 40, 50, 60, 70, 80, 90, 100, 200, 300, 400, 500, 600, 700, 800, 900, 1000 MeV/n) of ^{1}H, ^{2}H, ^{3}He, ^{4}He, ^{11}B, ^{12}C, ^{14}N, ^{16}O, ^{18}F, ^{20}Ne, ^{40}Ar, ^{56}Fe, ^{58}Ni, ^{84}Kr, ^{132}Xe and ^{238}U ions impinging on spheres of liquid water with diameter equal to 0.464 and 1 µm were simulated. The simulation cutoff was set to 1 keV/n for all ions. The stopping power values needed for both the computation of the lineal energy spectra with the PHITS microdosimetric analytical function and to calculate the ion energy loss were assessed with the ATIMA model (http://web-docs.gsi.de/~weick/atima) implemented in PHITS. A logarithmic binning from 10^{-3} to 10^{7} keV/µm with 50 bins per decade was used. The minimum energy deposition considered in the calculations with [T-SED] was the one relative to one event of one ionization only (~10 eV). The diameter of simulated site was changed accordingly to the requirements of the employed model, being 0.464 µm for the modified MKM and 1 µm for the BWF and IBWF approaches (more information can be found in Section 2.2 of this article).

The dose-mean lineal energy ($\bar{y}_D$) was calculated as in Equation 1 (International Commission on Radiation Units and Measurements, 1983) , where *d(y)* is the dose density distribution of the lineal energy *y* in keV/µm.

$$\bar{y}_D = \int_0^{+\infty} y\, d(y)\, \mathrm{d}y \quad (1)$$

The LET in water was evaluated in the same computational domains using the PHITS [T-LET] tally. In this case, the unrestricted dose density distributions of the primary beam LET was assessed as function of the LET in a logarithmic binning from 10^{-2} to 10^{6} with 50 bins per decade. Finally, the dose- mean LET ($\overline{LET}_{\mathrm{D}}$) values were calculated using Equation 2, where *d(LET)* represents the primary-beam dose- probability density of the LET as function of the LET in keV/μm. The primary $\overline{LET}_{\mathrm{D}}$ was assessed to ease the comparison between the results of the simulations and the *in vitro* data from the PIDE database (see paragraph 2.2.1), reported as a function of this quantity.

$$\overline{LET}_D = \int_0^{+\infty} LET\, d(LET)\, \mathrm{d}LET \quad (2)$$

2.2. Biophysical modeling

2.2.1. Experimental clonogenic survival data

The experimental data needed for the benchmark of the biophysical models (modified MKM and BWF) and for the development of the IBWF were extracted from the Particle Irradiation Data Ensemble (PIDE, Friedrich et al., 2013) version 3.1. Because of their widespread utilization and representing by far the biggest dataset in PIDE, the cell survival curves of the normoxic unsynchronized V79 cell line (Chinese hamster lung fibroblast) were used in this study. The obtained dataset includes 267 data points from 34 publications (Aoki et al., 2000, Belli et al., 1998, Belli et al., 2008, Bird and Burki, 1975, Blomquist et al., 1993, Böhrnsen et al., 1993, Britten et al., 2013, Cox et al., 1977a, Cox et al., 1977 b, Doria et al., 2012, Folkard et al., 1989, Folkard et al., 1996, Furusawa et al., 2000, Furusawa et al., 2002, Gerelchuluun et al., 2015, Hall et al., 1972, Hall et al., 1977, Hirayama et al., 2009, Jenner et al., 1993, Jeynes et al., 2013, Perris et al., 1986, Prise et al., 1990, Raju et al., 1991, Scholz, 2003, Schuff et al., 2002, Stenerlöw et al., 1995, Thacker et al., 1979, Tilly, 1999, Weber and Flentje, 1993, Wouters et al., 1996, Wouters et al., 2015, Wulf et al., 1985, Zhou et al., 2006) for 16 ions (^{1}H, ^{2}H, ^{3}He, ^{4}He, ^{11}B, ^{12}C, ^{14}N ^{16}O, ^{18}F, ^{20}Ne, ^{40}Ar, ^{56}Fe, ^{58}Ni, ^{84}Kr, ^{132}Xe and ^{238}U) spanning over a LET range from approximately 1 to 15000 keV/µm. Each data point is composed by the following quantities: the primary-beam unrestricted dose-mean LET ($\overline{LET}_{\mathrm{D}}$), the linear and the quadratic terms of the survival curve fitted using the linear quadratic model (McMahon, 2018) in case of ion exposure (respectively α and β) and for the reference photon exposure (α_{ref} and β_{ref}).

The RBE was assessed using Equation 3 (adapted from Hawkins, 1994) where S is the surviving fraction used in the calculations (10% in this study).

$$RBE\ (S) = \frac{\alpha + \sqrt{\alpha^2 - 4\,\beta\,\ln(S)}}{\alpha_{\mathrm{ref}} + \sqrt{\alpha_{\mathrm{ref}}^2 - 4\,\beta_{\mathrm{ref}}\,\ln(S)}} \qquad (3)$$

2.2.2. Modified microdosimetric kinetic model – modified MKM

The original microdosimetric kinetic model (MKM, Hawkins, 2003) was modified by Kase et al., 2006 by introducing in its formalism the concept of saturation corrected lineal energy (International Commission on Radiation Units and Measurements, 1983) to account for the overkill effect. The linear term of the linear quadratic model (α) can be assessed using Equation 4 (Kase et al., 2006)

$$\alpha = \alpha_0 + \beta_{\text{ref}} \bar{z}^*_{1D,d} \tag{4}$$

where α_0 is a constant representing the initial slope of the survival curve in the limit of $LET \rightarrow 0$, β_{ref} is the quadratic term of the linear quadratic model in case of the reference photon exposure and $\bar{z}^*_{1D,\,d}$ is the single-event saturation-corrected dose-mean specific energy in the domain. The latter quantity can be obtained as in Equation 5 where ρ_d, r_d and y_0 are respectively the density (= 1.0 g/cm³) and the radius of the domain, and the saturation parameter.

$$\bar{z}^*_{1D,d} = \frac{1}{\rho_d \pi r_d^2} \frac{y_0^2 \int_0^{+\infty} \left[1 - \exp\left(-\frac{y}{y_0}\right)\right] f(y)\, dy}{\int y\, f(y)\, dy} \tag{5}$$

Having assessed α and under the assumption that β term of the linear quadratic model is equal to β_{ref} independently from the radiation quality (Kase et al., 2006), the RBE was calculated as in Equation 3. In this work, we used the numerical values of the modified MKM parameters for V79 cells as previously determined by Sato et al., 2011, namely α_0 = 0.105 Gy^{-1}, α_{ref} = 0.184 Gy^{-1}, β_{ref} = 0.02 Gy^{-2}, r_d = 0.232 µm, and y_0 = 133.1 keV/µm.

2.2.3. Biological weighting function – BWF

The BWF approach is a biophysical model based on the idea of using single-event microdosimetric spectra to describe and predict the RBE of different radiation fields. The model was initially developed for intercomparing clinical cancer radiotherapy beams and during the years it has been widely employed in combination with experimentally-measured or computer-simulated microdosimetric spectra (i.e. Morstin et al., 1989, Pihet et al., 1990, Loncol et al., 1994, Paganetti et al., 1997, Brenner and Zaider, 1998, Pihet and Menzel, 1999, De Nardo et al., 2004 b, Conte et al., 2019, Zhu et al., 2019, Colautti et al., 2020).

According to the model formalism, it is hypothesized that the biological endpoint of interest can be calculated as the integral between the dose distribution of the lineal energy *d(y)* and a lineal energy weighting function *r(y)* called BWF (Equation 6). The modelled endpoint depends on the BWF chosen for the calculations.

$$RBE = \int_0^{+\infty} d(y)\, r(y)\, \mathrm{d}y \tag{6}$$

The most frequently used BWF was determined by Loncol et al., 1994 through an unfolding procedure on a dataset of combined exposures of spherical tissue equivalent proportional counters (TEPCs) and biological exposures to photons, neutrons and protons. The biological endpoint chosen was the mice intestine tolerance assessed by *in vivo* crypt regeneration for a 8 Gy exposure. The determined BWF is plotted in Figure 1 (solid line) as function of the lineal energy *y* in keV/µm. Because the original BWF was provided only up to a maximum lineal energy value of 1000 keV/µm (Loncol et al., 1994), a logarithmic extrapolation (best fit between 300 and 1000 keV/µm, dotted line in Figure 1) of the function was performed down to its intercept with the horizontal axis. In addition, because the BWF was assessed using TEPCs filled with a tissue-equivalent propane-based mixture, the lineal energy spectrum used for the RBE calculations should be in principle evaluated in the latter medium. However, because the average ratio between the mass stopping power values of the aforementioned gas mixture and liquid water is 1.0 in the energy/particle range of interest (according to the SRIM software version 2013.00, Ziegler et al., 2010), the BWF of Loncol et al., 1994 can be unchangingly applied also to the simulated lineal energy spectra in liquid water.

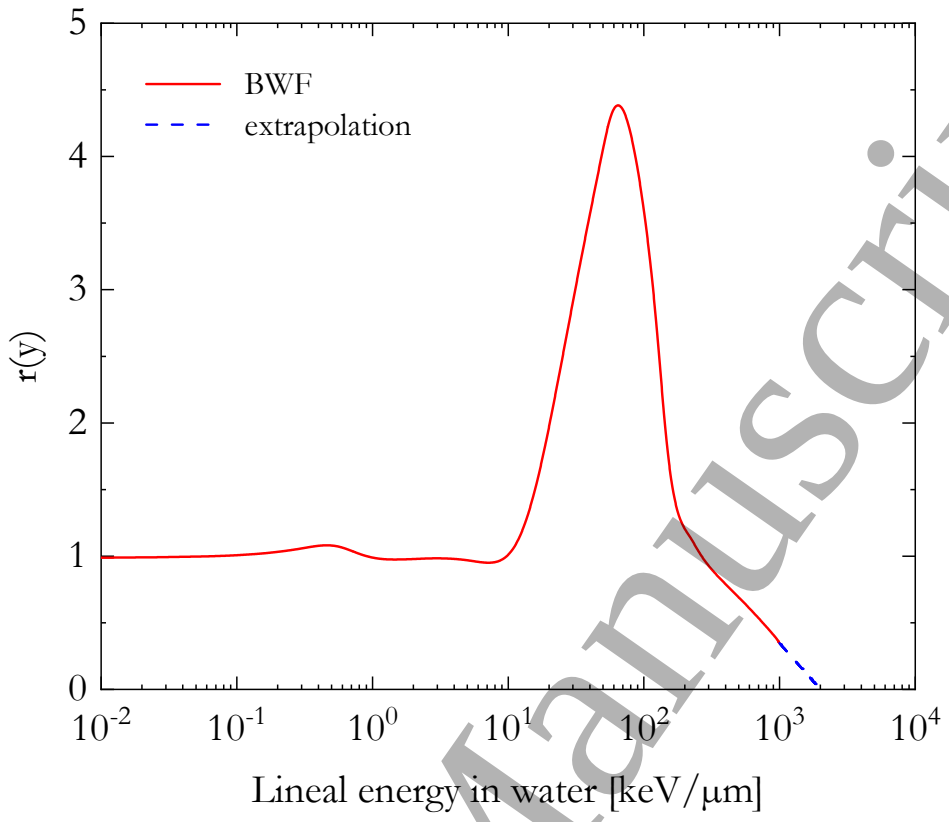

Figure 1. Biological weighting function (BWF) for the mice intestine tolerance assessed by crypt regeneration (Loncol et al., 1994, red solid line) and the extrapolation used in this study (blue dashed line).

2.2.4. Assessment of the improved biological weighting function – IBWF

As the same manner as the methodology described in the previous BWF paragraph, it is hypothesized that it is possible to establish a unique correlation between the RBE for a surviving fraction of 10% and the microdosimetric lineal energy spectra. The assessment of the optimal IBWF was then performed through an iterative process aimed to minimize the deviation between calculated RBE values and all experimental data for V79 cells extracted from the PIDE database. The 592 PHITS-simulated microdosimetric spectra for a target diameter of 1 µm (37 energies, 16 ions, see paragraph 2.1) were imported in MATLAB 2016b (The MathWorks inc., United States of America), folded into a temporary weighting function and the RBE calculated using Equation 6. The results were then compared to the $n = 267$ experimental points and the agreement between the latter ones and the model results was quantified as the average of the relative deviation $\bar{R}$ (Equation 7) over all ion species. RBE_{exp} and RBE_{IBWF} represent the experimentally assessed and calculated RBE_{10} values respectively.

$$\bar{R} = \frac{1}{n}\sum_{i=1}^{n}\frac{\left|RBE_{\mathrm{exp}} - RBE_{\mathrm{IBWF}}\right|}{RBE_{\mathrm{exp}}} \quad (7)$$

Because of their relevance for cancer radiotherapy, data relative to protons and carbon ions were given a double weight in respect to all other ions. The process was then repeated slightly changing the weighting function in order to minimize the average relative deviation. The process was stopped once the minimum value of the average relative deviation was found.

2.3. Application of the IBWF to experimentally measured microdosimetric spectra

The IBWF for the V79 cell line was determined by correlating the PHITS-simulated lineal energy spectra in 1 μm spherical volume with the *in vitro* RBE_{10} extracted from a database of survival data. It is not straightforward nor immediately assured that the same IBWF could reliably work also in combination with microdosimetric spectra measured with detectors which sensitive volume is made of different materials (i.e. gas, silicon, diamond) and possesses different shapes (i.e. cylinder, slab) or dimensions. To preliminarily investigate this point, the IBWF was unchangingly used to calculate the RBE_{10} by processing published microdosimetric spectra acquired with different detectors in clinical ^{1}H and ^{12}C beams, namely: a commercially available spherical TEPC filled with a propane-based tissue-equivalent gas mixture (Far West LET-1/2, http://www.fwt.com/detector/let1_2ds.htm), a cylindrical TEPC filled with a methane-based tissue-equivalent gas mixture (Gerlach et al., 2002), miniaturized cylindrical TEPCs filled with pure propane or a propane-based tissue-equivalent gas mixture (mini-TEPC, De Nardo et al., 2004 a, Conte et al., 2019), a wall-less TEPC filled with a propane-based tissue-equivalent gas mixture (Tsuda et al., 2010), an avalanche-confinement TEPC filled with dimethyl ether (Bortot et al., 2017), a synthetic diamond detector (Verona et al., 2015), the silicon-on-insulators microdosimeters MicroPlus Bridge (Tran et al., 2015) and MicroPlus Mushroom (Tran et al., 2017 b). The assessed RBE values were then correlated with the experimentally measured dose-mean lineal energy ($\bar{y}_D$, Equation 1) and the obtained RBE-vs-$\bar{y}_D$ trends were compared with the corresponding ones calculated by using PHITS-simulated spectra. For all detectors, only in-field measurements were considered in this work. More details on the measurement campaigns (irradiation facility, ion, maximum energy, dose profile, beam delivery modality, energy degradation system, references) are given in Table 1.

The sensitive volumes present relevant differences between the different microdosimeters. For the gas-based detectors, the simulated site size at unity density was 0.5 μm for the avalanche-confinement TEPC, 0.72 μm for the wall-less TEPC, 0.85 μm for the mini-TEPC at CATANA and CNAO, 1 μm for the Far West LET-1/2 TEPC and the cylindrical TEPC and 1.1 μm for the mini-TEPC at CAL. On the other hand, the sensitive volume of the diamond detector has a 200 x 200 μm^2 planar section and a thickness of 2 μm. The MicroPlus

silicon detectors are characterized by arrays of sensitive volumes with the shape of 30x30 μm^2 planar slabs with a thickness of 10 µm (MicroPlus Bridge) or of cylinders with diameter of 30 µm and a thickness of 9.1 µm (MicroPlus Mushroom). No corrections were performed to take into account the different chord length distributions of the sensitive volumes of the detectors. Furthermore, for the detector-beam combinations included in this study (10 µm thick silicon detectors in ^{1}H and ^{12}C beams and thin diamond detector in ^{12}C ion beams), the uncertainty arising from the lowest detectable lineal energy in solid-state detector was assumed to be negligible. On the other hand, in case of measurements with thin solid state detectors (i.e. 1-2 µm) in ^{1}H ion beams, this assumption would not hold and corrections would be needed.

As discussed in paragraph 2.2.3, no conversion factors were applied to convert to water the lineal energy distributions evaluated with detectors filled by a tissue-equivalent gas mixtures. On the other hand, the published spectra acquired with the diamond detector were converted to an equivalent propane cylindrical detector and then linearly scaled to obtain a carbon edge value corresponding to the one for water (more details can be found in Magrin et al., 2019). For the MicroPlus measurements at HIAF, MGH and HIMAC (the first two ones with the MicroPlus Bridge and the last one with the MicroPlus Mushroom), fixed conversion factors were employed to convert the microdosimetric spectra from silicon to water following the methodology described in Bolst et al., 2017. The microdosimetric measurements with the MicroPlus Mushroom at OCL were converted using the energy-dependent correction function described in Samnøy et al., 2020. Finally, the MicroPlus Bridge spectra measured at CCB IFJ PAN were converted bin-per-bin from silicon to water in a similar way as done in Magrin et al., 2019 for the diamond detector.

Table 1. Overview of the experimental microdosimetric spectra used for the RBE calculation in combination with the IBWF.

Detector	Ion	Maximum energy [MeV/n]	Dose profile	Irradiation facility	Delivery modality	Energy degradation	Reference
Avalanche-confinement TEPC	^{1}H	62	SOBP	CATANA	Passive	PMMA	Mazzucconi et al., 2019
Far West LET-1/2 TEPC	^{1}H	155	Monoenergetic	PMRC	Passive	Water	Kase et al., 2013
Far West LET-1/2 TEPC	^{1}H	155	SOBP	PMRC	Passive	Water	Kase et al., 2013
MicroPlus Bridge	^{1}H	131	Monoenergetic	MGH	Scanning	Water	Tran et al., 2017 a
MicroPlus Bridge	^{1}H	137	SOBP	MGH	Passive	Water	Tran et al., 2017 a
MicroPlus Bridge	^{1}H	60	Monoenergetic	CCB	Passive	Water	SCK CEN unpublished data
MicroPlus Mushroom	^{1}H	15	Monoenergetic	OCL	Passive	Polyamide	Samnøy et al., 2020
mini-TEPC	^{1}H	65	SOBP	CAL	Passive	PMMA	De Nardo et al., 2004 b
mini-TEPC	^{1}H	62	SOBP	CATANA	Passive	PMMA	Conte et al., 2019
Wall-less TEPC	^{1}H	160	Monoenergetic	HIMAC	Passive	PMMA	Tsuda et al., 2012
Avalanche-confinement TEPC	^{12}C	195	Monoenergetic	CNAO	Scanning	PMMA	Bortot et al., 2020
Cylindrical TEPC	^{12}C	430	Monoenergetic	GSI	Passive	PMMA	Gerlach et al., 2002
Diamond detector	^{12}C	195	Monoenergetic	CNAO	Scanning	Water	Magrin et al., 2019
Far West LET-1/2 TEPC	^{12}C	290	Monoenergetic	HIMAC	Passive	Water	Kase et al., 2011
MicroPlus Bridge	^{12}C	6	Monoenergetic	HIAF	Passive	LDPE	Tran et al., 2015
MicroPlus Mushroom	^{12}C	290	Monoenergetic	HIMAC	Passive	Water	Tran et al., 2018
mini-TEPC	^{12}C	295	Monoenergetic	CNAO	Scanning	Water	Conte et al., 2017
mini-TEPC	^{12}C	62	SOBP	CATANA	Passive	PMMA	Colautti et al., 2018
Wall-less TEPC	^{12}C	290	Monoenergetic	HIMAC	Passive	N/A	Tsuda et al., 2010

3. Results

3.1. Simulated microdosimetric lineal energy spectra

The PHITS-simulated lineal energy *yd(y)* spectra in case of selected ions (^{1}H, ^{4}He, ^{12}C, ^{20}Ne, ^{56}Fe, ^{132}Xe and ^{238}U) and energies (1, 10, 100 and 1000 MeV/n) are plotted in Figure 2 for both microdosimetric site sizes included in this study (0.464 and 1 μm diameter). The calculated dose probability density distributions are characterized by a shift to higher lineal energy values with the decrease of the incident particle energy, due to the well-known increase in the density of energy deposition (i.e. the stopping power) at low energy. However, it must be noted that in case of ^{238}U ions the microdosimetric spectra relative to 10 MeV/n present an edge located at higher lineal energy values than the one for 1 MeV/n ^{238}U ions. This is due to the fact that, differently from all other particles included in Figure 2, the stopping power of ^{238}U ions with energy equal to 10 MeV/n is higher than the one for 1 MeV/n. In this regard, Figure 3 compares the total stopping power in liquid water of ^{1}H, ^{4}He, ^{12}C, ^{20}Ne, ^{56}Fe, ^{132}Xe and ^{238}U ions as a function of the particle energy between 0.001 and 1000 MeV/n. The stopping power values were calculated using the Stopping and Range of Ions in Matter (SRIM, Ziegler et al., 2010) version 2013.00. As it can be seen, the maximum value of the particle stopping power over the investigated energy range gradually moves to higher energies with the increase of the atomic mass number of the incident particle, i.e. around 0.08 MeV for ^{1}H ions, around 0.3 and 0.8 MeV/n for respectively ^{12}C and ^{56}Fe ions, and finally at approximately 6 MeV/n for ^{238}U ions. Finally, deviations between the spectra induced in the two different site sizes (0.464 and 1 μm diameter) are more evident in case of lighter ions, with the spectra relative to a site of 0.464 μm diameter being broader than the corresponding ones in case of the sphere with 1 μm diameter due to the increased fluctuations in the energy deposition with the decrease of the target size and the increased contribution of δ-rays acting as touchers (i.e. liberated outside the target volume, Caswell and Coyne, 1989).

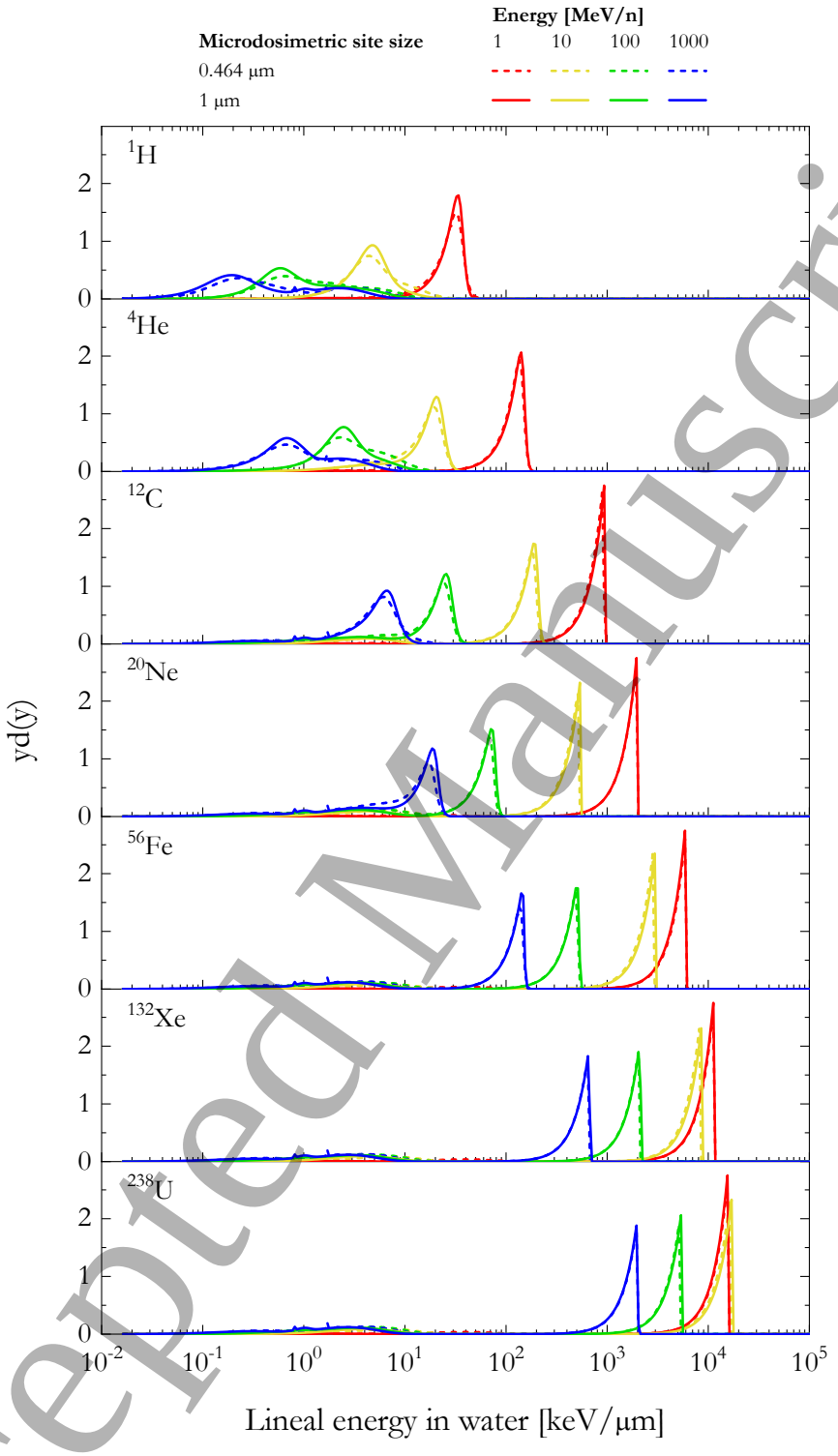

Figure 2. PHITS-simulated lineal energy spectra for selected particles (^{1}H, ^{4}He, ^{12}C, ^{20}Ne, ^{56}Fe, ^{132}Xe and ^{238}U) and energies (1, 10, 100 and 1000 MeV/n).

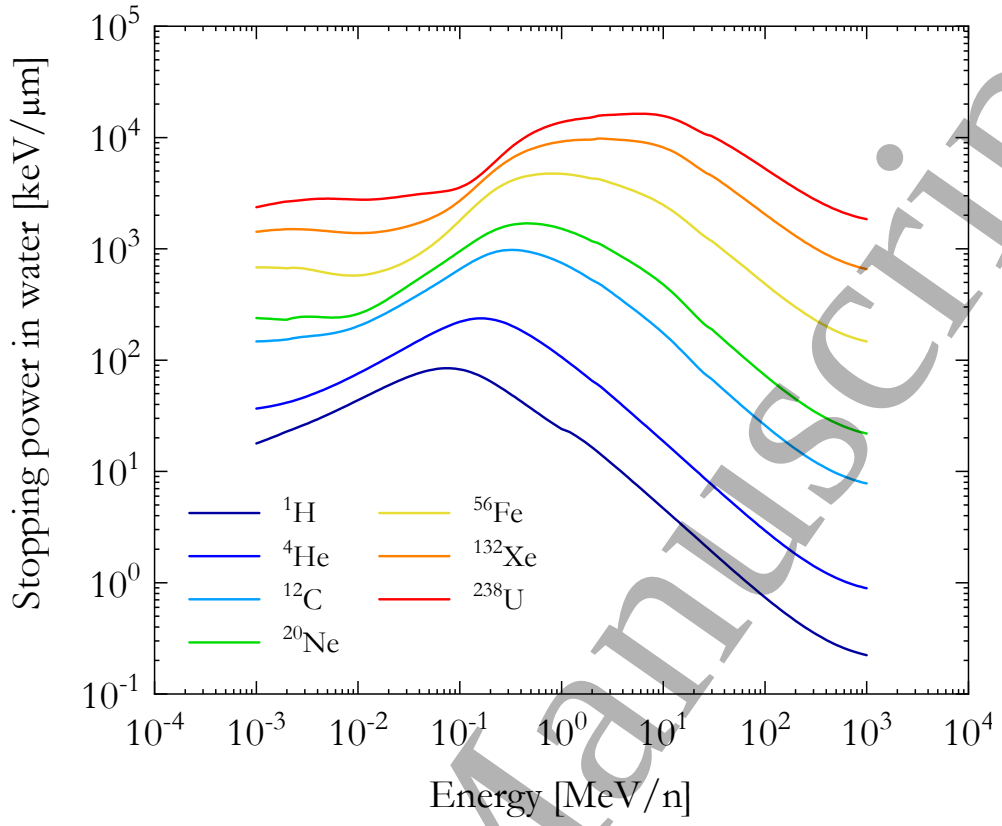

Figure 3. Total stopping power of ^{1}H, ^{4}He, ^{12}C, ^{20}Ne, ^{56}Fe, ^{132}Xe and ^{238}U ions as a function of the particle energy. The values were calculated using SRIM version 2013.00 (Ziegler et al., 2010).

3.2. Determination of the IBWF for the V79 cell line

As an example of the results of the iterative process which led to the determination of the IBWF for the V79 cell line, Figure 4 shows the effect of varying and co-varying up to ±20% the horizontal (rigid translation of the function of Figure 5 towards higher/lower lineal energy values) and vertical (rigid translation of the values of function of Figure 5, equivalent to multiplying the function with a constant value) position of the optimal IBWF (Figure 5) on the average relative deviation between calculated and experimental values. The optimal IBWF, corresponding to the local minimum at 14.4% is plotted in Figure 5 in comparison to the Loncol's BWF. In the plotted interval, variations in the horizontal position of IBWF seem to affect the calculated average relative deviation in a minor way in respect to variations in its vertical position. In the first case, the maximum deviation was found to be 17.0% for a -20% negative shift in the horizontal position of the IBWF. On the other hand, the maximum value of the average relative deviation due to vertical shifts of the IBWF was observed in case of a +20% translation, being 25.2%. The maximum disagreement between calculated and experimentally measured RBE_{10} values was assessed to be 28.3% for a combined variation of horizontal and vertical IBWF positions of respectively -20% and +20%.

The IBWF (Figure 5) is similar in shape to the Loncol's BWF, being characterized by a flat profile around 1 followed by a local maximum and a decrease. However, the IBWF's increase is less sharp than the BWF one and starts at lower lineal energy values (approximately 1 instead of 10 keV/µm). The IBWF maximum is located at 134 keV/µm, almost the double than for the BWF. It is worth noticing that the aforementioned lineal energy value of the IBWF turning point (defining the onset of the cell-damaging saturation due to overkill effects) is very similar to the saturation parameter of the modified MKM in case of the V79 cell line (y_0 = 133.1 keV/µm) as previously reported in Sato et al., 2011.

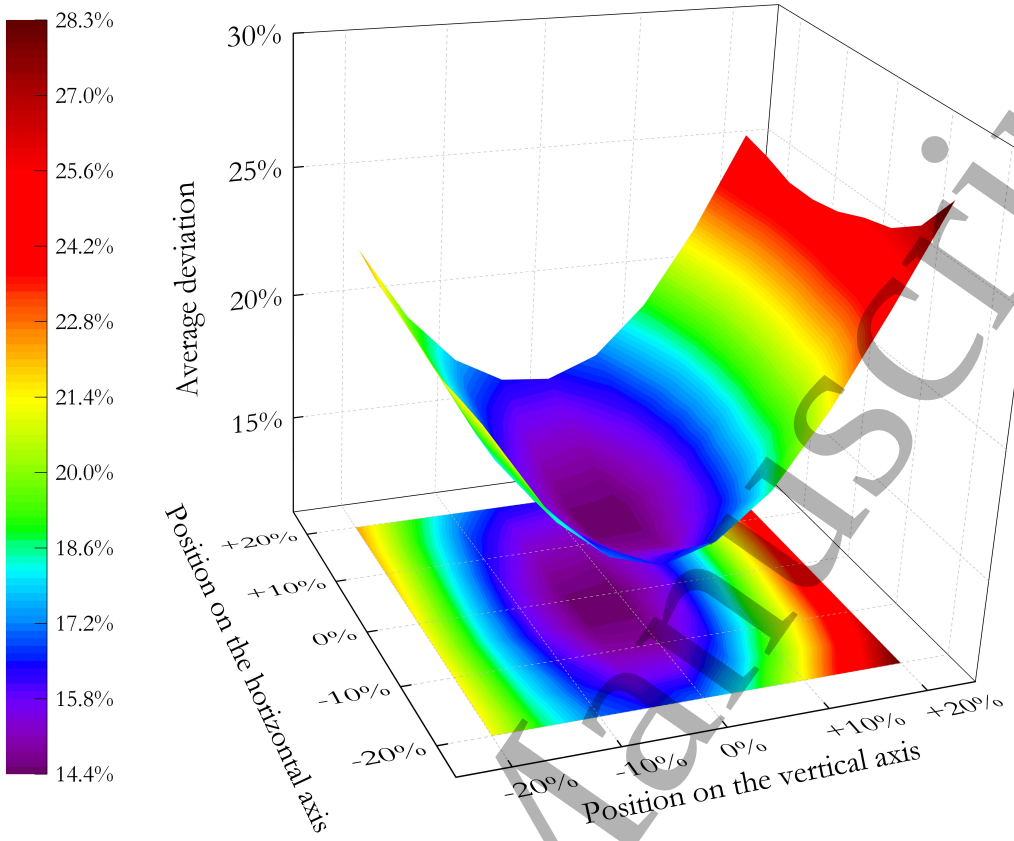

Figure 4. Effect of varying and co-varying the position of the IBWF on the average relative deviation between calculated and experimentally determined RBE_{10} values for the V79 cell line.

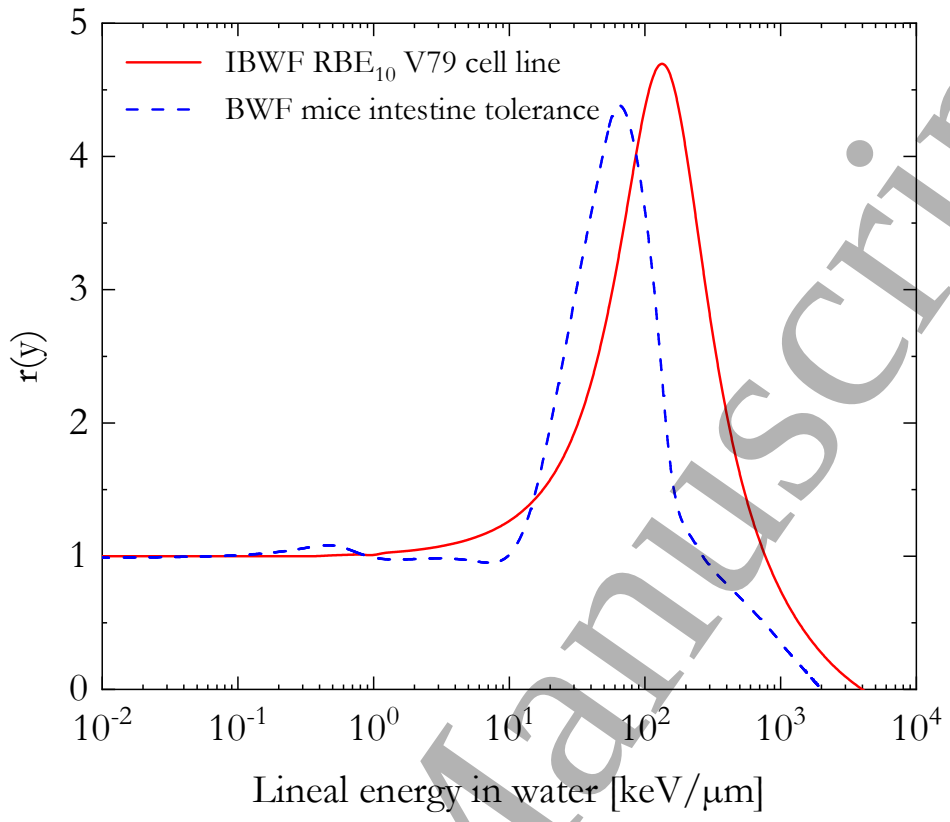

Figure 5. The improved biological weighting function (IBWF) for the *in vitro* RBE_{10} of the V79 cell line. The BWF for the *in vivo* early intestine tolerance (Loncol et al., 1994) was included for comparison.

3.2. Comparison between the biophysical models and *in vitro* data

Using the PHITS-simulated microdosimetric spectra (for the sites with 0.464 and 1 μm diameter) in combination with MKM, the BWF or the IBWF, the RBE (*in vitro* RBE_{10} in case of the V79 cell line for the IBWF and the modified MKM or the *in vivo* early intestine tolerance for the BWF) was assessed for ions from ^{1}H to ^{238}U and compared with the *in vitro* experimental V79 RBE_{10} data from the PIDE database. These results are plotted in Figure 6 as a function of the dose-mean LET for the 16 ion types included in this study. The agreement between the experimental *in vitro* RBE_{10} and the corresponding values calculated with the modified MKM and the IBWF was quantified using Equation 7 for each ion specie and the results are plotted in Figure 7 as a function of the atomic mass number of the particle. Only as a measure of the correlation between the BWF results and the *in vitro* RBE data, Figure 7 also reports the relative deviation between these two data series.

Furthermore, the RBE_{10} values calculated using the IBWF approach are summarized in Figure 8 as a function of the dose-mean LET for selected ions (^{1}H, ^{3}He, ^{12}C, ^{20}Ne, ^{40}Ar, ^{58}Ni, ^{84}Kr, ^{132}Xe, ^{238}U) in comparison to experimental data. The general trend of the RBE_{10} as a function of the LET consists in an initial increase until a maximum value located at around 100-200 keV/μm, followed by a decrease at higher LET. However, it is immediately noticed that the calculated RBE_{10} is not a unique function of the LET, but depends strongly also on the particle type. As an example, for ^{3}He, ^{12}C, ^{20}Ne and ^{40}Ar ions with a LET of 100 keV/μm, the RBE_{10} values strongly differ one from the other, being respectively 4.1, 3.3, 3.1 and 2.8. Finally, for a better visualization of the agreement between IBWF results and the experimental data in case of the four heaviest ions (^{58}Ni, ^{84}Kr, ^{132}Xe and ^{238}U), Figure 9 represents a detailed view of the RBE_{10} in this very high LET region.

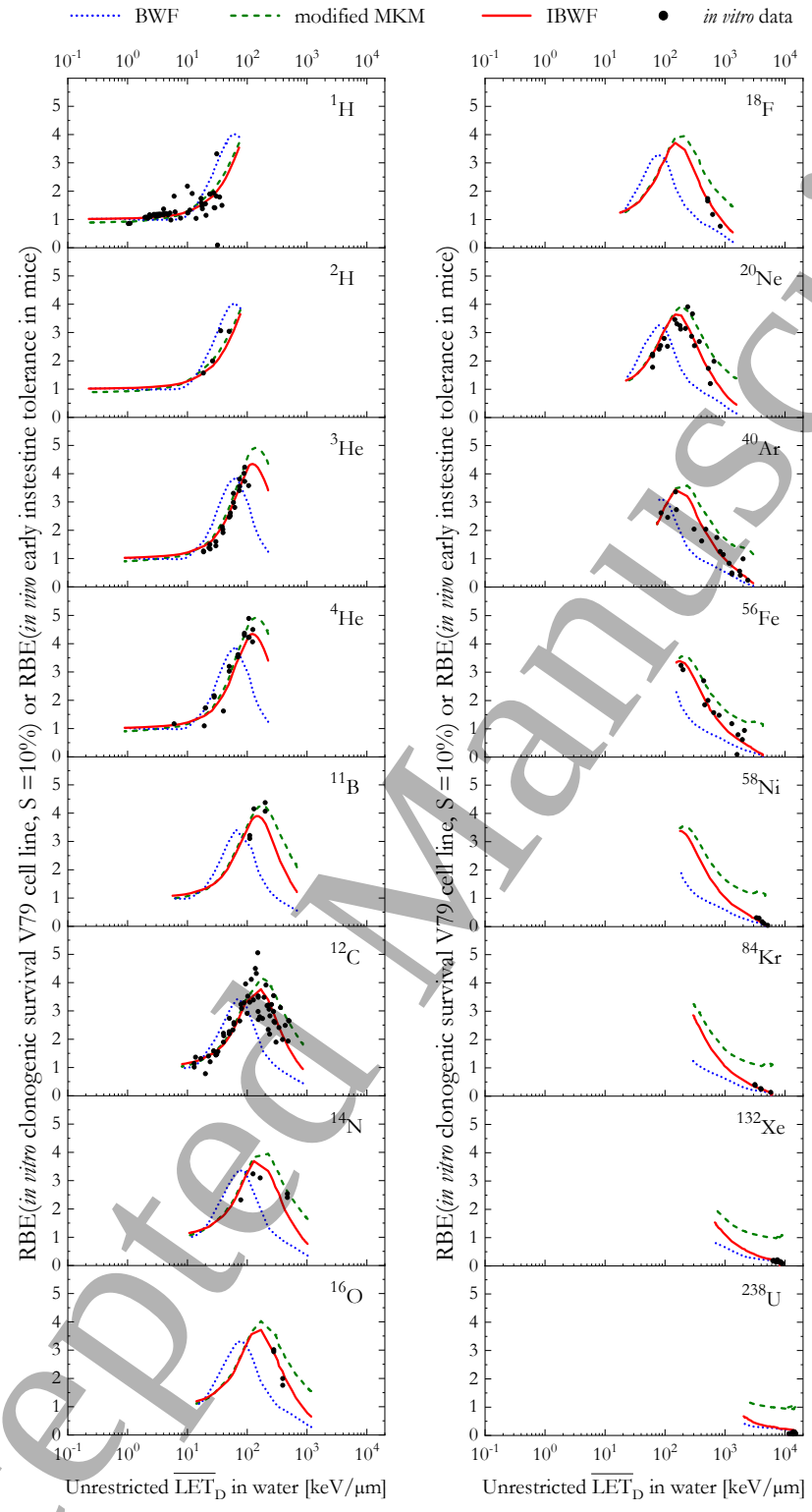

Figure 6. RBE calculated by the three models in comparison with *in vitro* data for the V79 cell line exposed to ions from ^{1}H to ^{238}U.

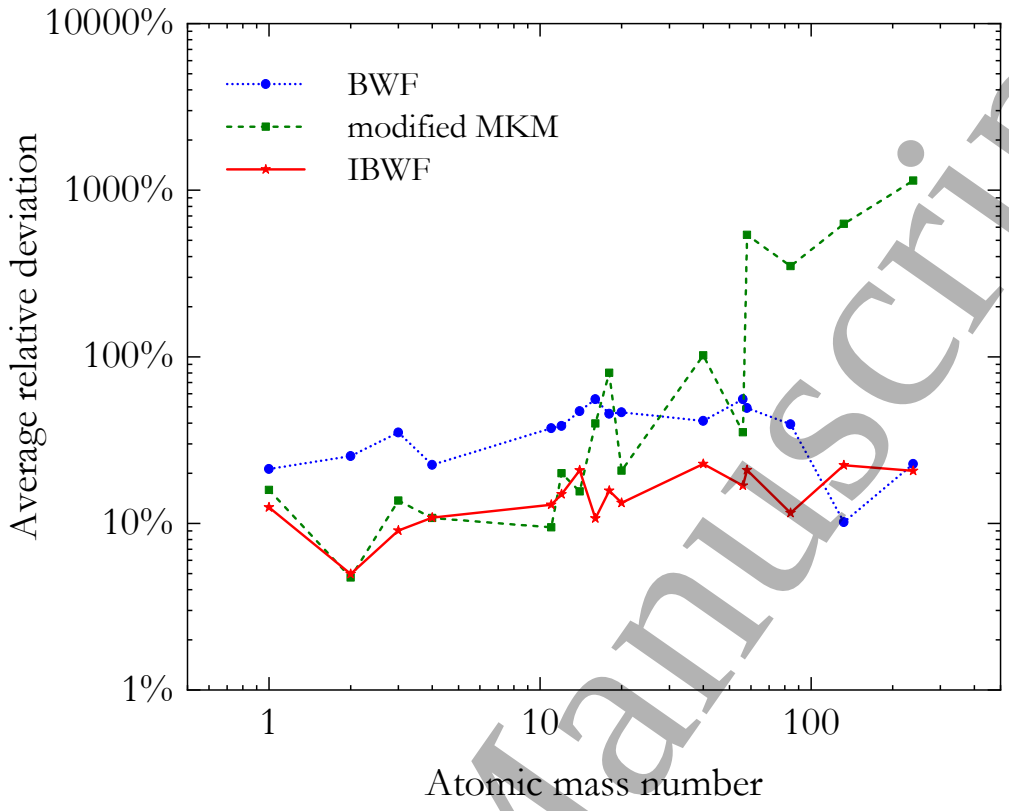

Figure 7. Average relative deviation between the results of the three biophysical models and the *in vitro* experimental data for the V79 cell line. For the BWF, these results are meant only as a measure of the correlation between its results and the *in vitro* data. The lines are just a guide to the eye.

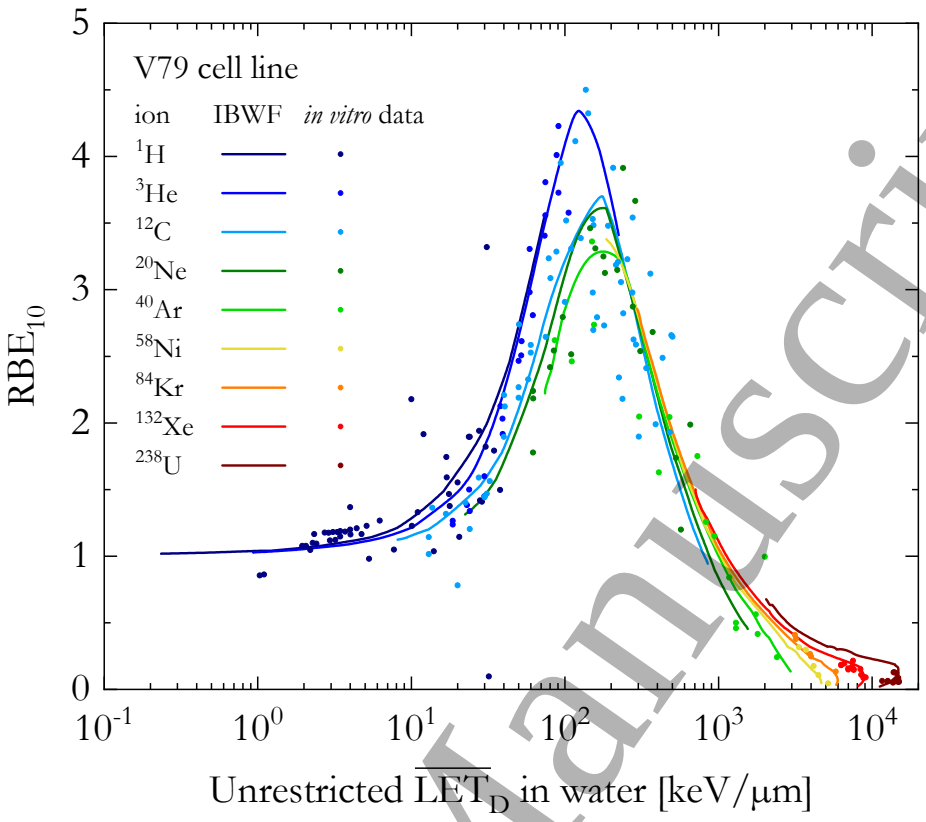

Figure 8. Overview of the RBE_{10} calculated by the IBWF (lines) for selected ions in comparison to *in vitro* data (dots) for the V79 cell line.

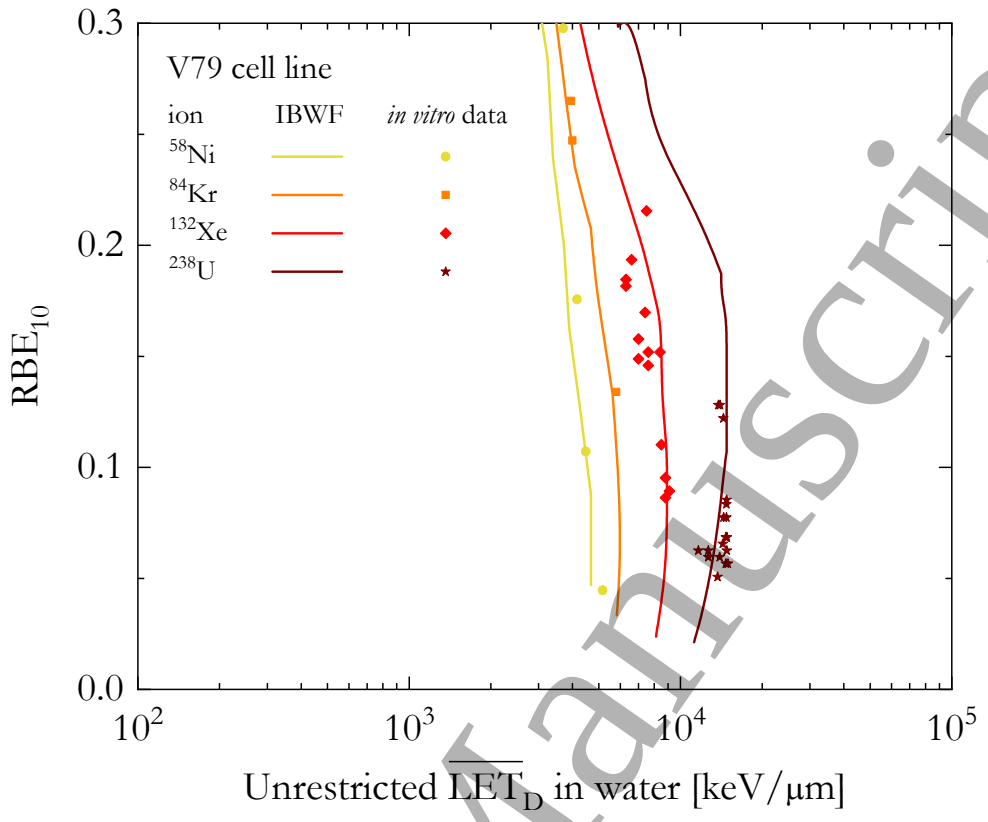

Figure 9. Detailed view of the RBE_{10} calculated by the IBWF (lines) in the very high LET range for ^{58}Ni, ^{84}Kr, ^{132}Xe and ^{238}U ions in comparison to *in vitro* data (dots) for the V79 cell line.

3.3. Application of the IBWF to experimentally measured microdosimetric spectra

The RBE_{10} values obtained by folding the IBWF into the experimentally-measured or PHITS-simulated spectra are plotted in Figures 10 and 11 as a function of the dose-mean lineal energy $\bar{y}_D$ for ^{1}H and ^{12}C ions respectively. In case of ^{1}H ions, because of the broader energy range of the PHITS simulations, the maximum computed RBE value was 3.5, higher than the maximum experimentally-based RBE counterpart (approximately 2.2). Nevertheless, a striking agreement between all RBE-vs-$\bar{y}_D$ trends is present in Figure 10, with the average relative deviation between the RBE_{10} values calculated processing PHITS-simulated or experimentally-measured spectra being 1.1% for the avalanche-confinement TEPC at CATANA (SOBP), 0.8% for the Far West LET-1/2 TEPC at PMRC (monoenergetic), 1.2% for Far West LET-1/2 TEPC at PMRC (SOBP), 0.7% for the MicroPlus Bridge at MGH (monoenergetic), 0.7% for the MicroPlus Bridge at MGH (SOBP), 0.8% for the MicroPlus Bridge at CCB (monoenergetic), 0.2% for the MicroPlus Mushroom at OCL (monoenergetic), 0.9% for the mini-TEPC at CAL (SOBP), 0.9% for the mini-TEPC at CATANA (SOBP) and 0.3% for the wall-less TEPC at HIMAC (monoenergetic). The average relative deviation between the RBE values obtained by using the experimental ^{1}H spectra and the corresponding ones computed with PHITS was assessed being 0.8%. Similarly for ^{12}C ions, a good agreement between the results of all data series is observable in Figure 11 (average relative deviation in respect to PHITS-based calculations = 5.7%). The latter value is higher than for ^{1}H ions because of the greater dose-contribution of the liberated secondary fragments in case of ^{12}C irradiations in combination with energy degrading systems. Furthermore, it is worth remembering that, in order to obtain the most-general applicable RBE dependencies, the PHITS simulations were performed in case of monoenergetic and monoparticle beams avoiding then the contamination due to fragments created upstream the target position during the particle slowing down. Nevertheless, with few exceptions in case of distal edge measurements, the experimentally-based results were found to lie within 10% from the PHITS-ones. The average relative deviation from the PHITS results was assessed being 2.5% for the avalanche-confinement TEPC at CNAO (monoenergetic), 2.8% for the cylindrical TEPC at GSI (monoenergetic), 11.8% for the diamond detector at CNAO (monoenergetic), 6.0% for the Far West LET-1/2 TEPC at HIMAC (monoenergetic), 5.5% for the

MicroPlus Bridge at HIAF (monoenergetic), 3.8% for the MicroPlus Mushroom at HIMAC (monoenergetic), 8.3% for the mini-TEPC at CNAO (monoenergetic), 11.2% for the mini-TEPC at CATANA (SOBP) and 1.1% for the wall-less TEPC at HIMAC (monoenergetic).

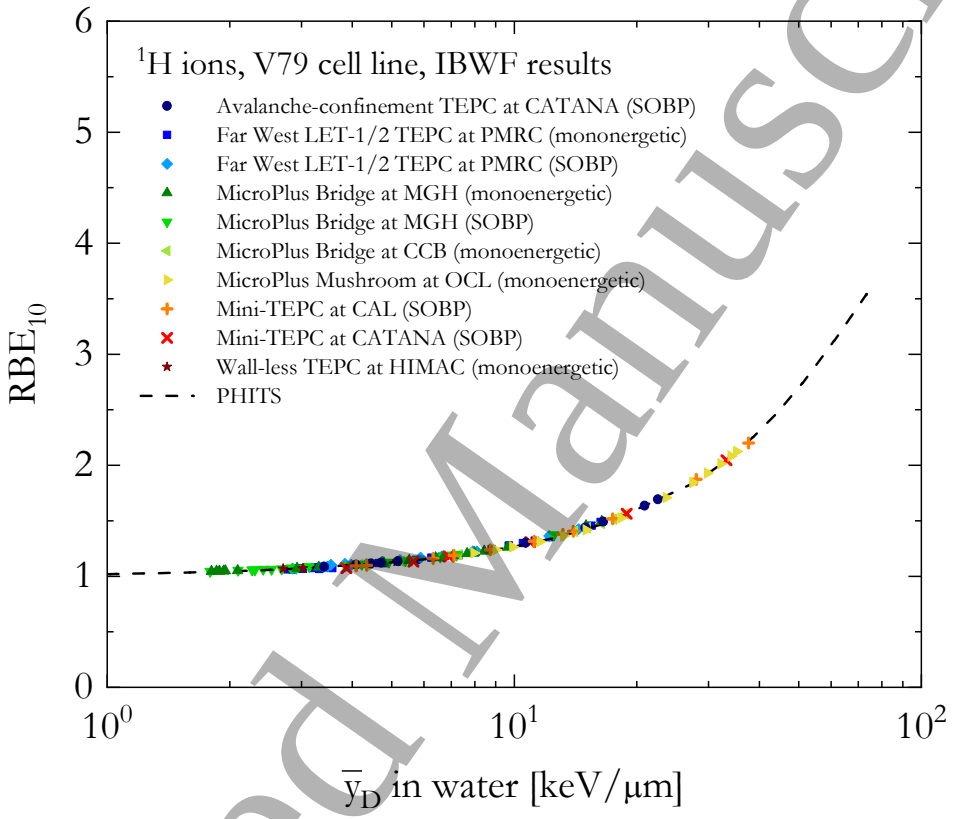

Figure 10. Comparison between the RBE-vs-$\bar{y}_D$ correlation obtained by combining the IBWF with experimentally-measured spectra in clinical ^{1}H facilities or PHITS-simulated spectra in case of monoenergetic ^{1}H beams.

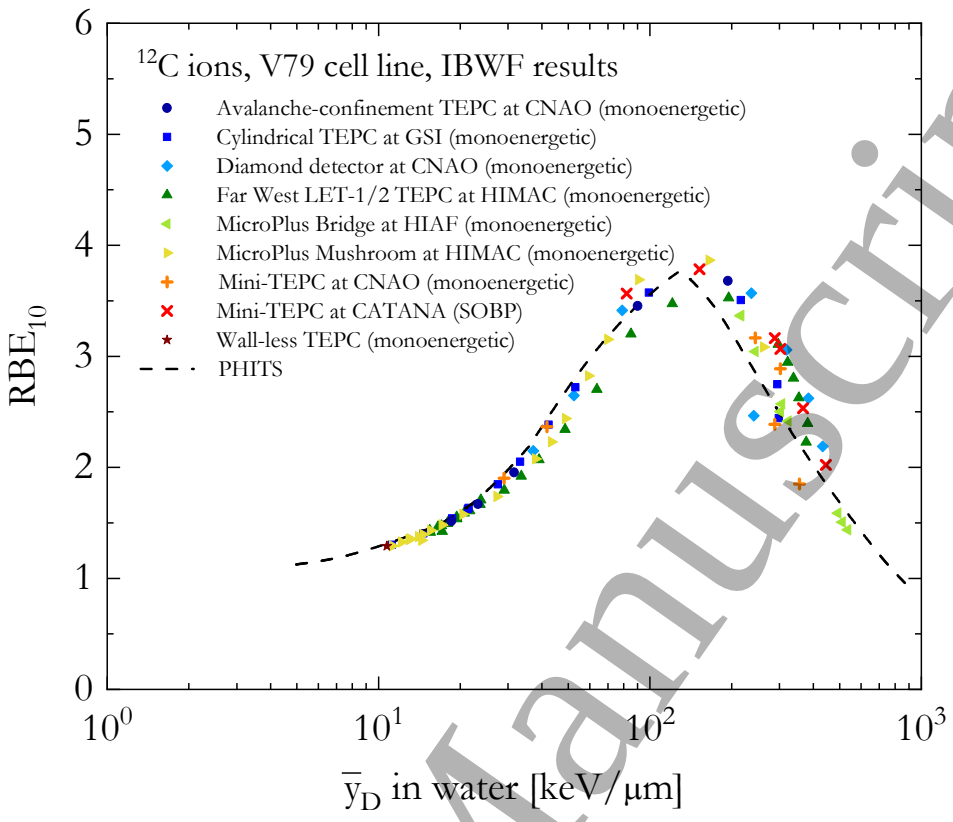

Figure 11. Comparison between the RBE-vs-$\bar{y}_D$ correlation obtained by combining the IBWF with experimentally-measured spectra in clinical ^{12}C ion facilities or PHITS-simulated spectra in case of monoenergetic ^{12}H beams.

4. Discussion

Using the Monte Carlo radiation transport code PHITS, 1184 microdosimetric lineal energy spectra were simulated in case of monoenergetic particle beams (ions = ^{1}H – ^{238}U, energy = 0.1 – 1000 MeV/n, unrestricted LET in liquid water = 0.2 – 15000 keV/µm) impinging on a water sphere with diameter equal to 0.464 or 1 µm. Similarly as in other models of radiation-action for solid state detectors (i.e. Olko et al., 2002, Parisi et al., 2019) and biological targets (i.e. Frese et al., 2012, Cunha et al., 2017, Friedland et al., 2017, McMahon et al., 2017), monoenergetic particle beams were chosen to derive particle-dependent results to be afterwards compared with the literature data generally plotted as a function of the particle energy or its LET. This was done in order to efficiently tackle the large variability of the *in vitro* data described in paragraph 2.2.1 of this article. The simulation of a specific experiment is out of the scope of this investigation. An additional advantage of the employed approach lies in the possibility of creating look-up tables reporting the relevant modelled quantity (i.e. the V79 RBE_{10} for this study) as a function of the particle type and the energy. Afterwards, these look-up tables can be used in more realistic scenarios in combination with the calculated particle spectra at cell position, removing thus the need for explicitly assessing the microdosimetric distributions and relevantly reducing the computational time.

The obtained density distributions were used in combination with the modified microdosimetric kinetic model (modified MKM, Kase et al., 2006, optimized parameters from Sato et al., 2011) or the biological weighting function (BWF, Loncol et al., 1994) to assess respectively the *in vitro* clonogenic survival RBE for the V79 cell line in case of a 10% surviving fraction or the *in vivo* early intestine tolerance in mice. The aforementioned microdosimetry-based biophysical models were chosen because of being the two most-commonly used ones in literature. In the first case, this was done in order to benchmark the performances of the modified MKM over a very broad particle-energy range. On the other hand, the BWF was employed for comparison purposes and to further explore potential correlations between the BWF results and the *in vitro* RBE as previously reported in case of proton exposures (De Nardo et al., 2004 b, Conte et al., 2019, Colautti et al., 2020). Furthermore, a phenomenological approach based on an improved biological weighting function (IBWF) was proposed to

investigate the possibility to establish a univocal correlation between simulated lineal energy spectra and the 10% cell survival of the V79 cell line. The obtained results were compared against 267 corresponding *in vitro* RBE_{10} data points for the V79 cell line from the PIDE database. The cell line was chosen because it represents the most abundant fraction in the database.

As it can be seen in Figure 6, the RBE_{10} values for the V79 cell line calculated using the modified MKM are found to well describe the corresponding *in vitro* experimental data up to ^{20}Ne ions. For heavier particles, the RBE_{10} values appears to be overestimated, with deviations up to ~1700% for ^{238}U ions (Figure 7). The average value of the relative deviation between experimental data and modified MKM calculations was assessed to be 76%. The findings suggest that for very-high LET exposures corrections and improvements to the modified MKM formalism are needed, i.e. by explicitly taking into account the stochastic nature of energy deposition in both the cell nucleus and in the subnuclear radiation-sensitive targets (Sato and Furusawa, 2012), including non-targeted effects (Sato and Hamada, 2014, Matsuya et al., 2018) or considering a variable β term (Chen et al., 2007, Inaniwa and Kanematsu, 2018).

Although a reasonable similarity between the results of BWF was observed for ^{1}H and ^{2}H ions, the BWF-calculated RBE values strongly differ from the V79 *in vitro* RBE_{10} ones from the PIDE database. This might be due to the different onset of the saturation behavior between the different endpoints, i.e. around 70 keV/μm for the *in vivo* early intestine tolerance and roughly the double for the *in vitro* RBE_{10} for the V79 cell line (Figure 5). The average deviation between these two data series (BWF results and PIDE) was found to be 33%.

On the other hand, the results of the IBWF model were able to reproduce well the PIDE *in vitro* data over the whole particle and energy range (average relative deviation = 14%) without adapting the weighting function to the different exposure conditions. Even in the very-high LET range (Figure 9) and notwithstanding the experimental uncertainty of the *in vitro* data, the values calculated by the IBWF well agree with the experimental data by means of four separate almost-parallel particle-specific RBE curves.

The proposed IBWF is not a predictive or an *ab initio* model, but a simple and robust tool for a fast RBE assessment to compare different exposure conditions. Consequently, its usage should be limited only for the calculation of the biological endpoint (*in vitro* 10% surviving fraction) and cell line (unsynchronized normoxic V79) employed for its determination. In case another system or endpoint should be modeled, it is suggested that other biophysical models should be used or alternatively a new weighting function should be developed. Especially for high dose or high LET exposures, a predictive model should consider the variations in the microdosimetric spectra as a function of the imparted dose (i.e. multi-event spectra, Brenner and Zaider, 1998), an effect which is consciously disregarded in the IBWF and other purely phenomenological approaches making use of biological weighting functions (Pihet and Menzel 1999).

Possible correlations between the IBWF results (RBE_{10}, V79 cell line) and the corresponding *in vitro* RBE_{10} values for other cell lines will be part of a separate investigation. Nevertheless, a preliminary comparison between the Chinese hamster lung fibroblast V79 proton RBE_{10} values of this work and the corresponding *in vitro* experimental results for the normal human fibroblast AG01522 (Chaudhary et al., 2014), human glioblastoma U87 (Chauduary et al., 2014), large cell human carcinoma H460 (Guan et al., 2015) and human lung adenocarcinoma H1437 (Guan et al., 2015) cell lines seems to indicate the presence of a similar RBE increase with the increase of the proton LET. Additionally, feasibility-studies are planned to explore the possibility of determining weighting functions by analyzing only a subset of the *in vitro* RBE data available (i.e. by fitting values relative to selected ions) or to model the α and ß term of the linear quadratic model as a function of indicators of the radiation sensitivity such as the α/ß ratio in case of the reference photon exposure. In this way, it might be possible to account for the dose-, endpoint and system dependence of the RBE.

Furthermore, the IBWF was here developed by processing microdosimetric spectra calculated in a site with 1 µm diameter, as done in precedent studies for similar BWFs and being 1 µm the most common simulated site size in gas-based microdosimeters. Nevertheless, although representative of the dimension of chromosomic territories and the clustering of DNA damages on a scale relevant for cell death, the choice of the 1 µm site size could be regarded as somehow arbitrary. Notwithstanding the minor deviations in the lineal energy spectra

between the targets with 0.464 and 1 μm diameter (Figure 3), the optimized IBWF could differ from the one plotted in Figure 5 if another microdosimetric site size was used for the calculations.

Finally, because its intercomparison-triggered nature, the IBWF was applied to calculate RBE values from the microdosimetric spectra experimentally measured with 8 different detectors in 19 pristine and spread out Bragg peaks of ^{1}H and ^{12}C beams at 8 clinical and 2 research facilities. It has to be underlined that the spectra were acquired with detectors having different geometries, dimensions and materials composing the sensitive volume. Furthermore, the exposure conditions (i.e. maximum beam energy, monoenergetic or SOBP dose profile, passively scattered or scanning delivery system, water/PMMA/LDPE/polyamide energy degradation, irradiation facility) strongly differed, as summarized in Table 1. In addition, the procedure employed to convert microdosimetric spectra from the detector material to water was not the same. Nevertheless, a very good and somehow surprising agreement was found between the RBE-vs-$\bar{y}_D$ trends determined using the different datasets (measurements or PHITS simulations), with an average deviation of 0.8% and 5.7% for ^{1}H and ^{12}C ions respectively. It appears clear that possible under- or over- estimations in the experimentally-determined $\bar{y}_D$ in respect to reference calculations for a water sphere of 1 μm diameter will impact also the assessed RBE in a similar way as for the modified MKM or the BWF. Consequently, in those cases it suggested to perform corrections in the experimental spectra (i.e. conversion of the spectra from the detector material and shape to spherical water sensitive volume as described in Magrin, 2018) or to employ a different microdosimeter whose measured spectra directly match more closely the PHITS-simulated ones. Alternatively, detector-specific biological weighting function taking into account the material and shape of the sensitive volume of the microdosimeters could be developed and used for the RBE assessment.

5. Conclusions

The accuracy of the modified MKM for modeling the 10% clonogenic survival of unsynchronized normoxic Chinese hamster lung fibroblasts (V79 cell line) was systematically tested against the PIDE *in vitro* database in case of exposures to ions from ^{1}H to ^{238}U spanning over a very large unrestricted LET in water range (0.2 – 15000 keV/μm). The model showed limitations in reproducing the *in vitro* data for ions heavier than ^{20}Ne and its usage is not recommended outside the indicated interval. Furthermore, the results suggest that the previously reported good correlation between Loncol's BWF calculations and *in vitro* RBE_{10} data in case of proton irradiations does not hold for particles heavier than ^{2}H ions.

In combination with PHITS-simulated microdosimetric spectra, an improved biological weighting function (IBWF) was determined through a global fit of the *in vitro* V79 data included in the PIDE database. The results proved the possibility to establish an univocal correlation between lineal energy spectra and the 10% clonogenic survival of the V79 cell line for all the investigated radiation qualities (average relative deviation with the *in vitro* data = 14%). Furthermore, a good agreement was found between the IBWF-based RBE-vs-$\bar{y}_D$ trends obtained by processing PHITS-simulated or experimentally-measured microdosimetric spectra acquired with 8 different detectors in different exposure scenarios (19 ^{1}H and ^{12}C beams at 8 clinical and 2 research facilities).

Thus, it is suggested that the IBWF could be regarded as a fast and easy-to-use tool for intercomparing clinical beams or the results acquired with different radiation detectors. Finally, the application of the IBWF for modeling other endpoints than the 10% clonogenic survival of the V79 cell line is currently discouraged as well as arbitrary rescaling of the function or of its results.

Acknowledgments

Alessio Parisi is very thankful to Thomas Friedrich for providing him access to the PIDE database and to the Research Foundation - Flanders (FWO) for the "Short stay outside Europe" grant to partly cover the expenses of his stay in Japan. Alessio Parisi thanks Shuichi Tsuda (Japan Atomic Energy Agency, Japan – currently at Nuclear Energy Agency, France), Davide Mazzucconi, Davide Bortot and Stefano Agosteo (Polytech of Milano, Italy) and Andreas Tefre Samnøy (University of Bergen, Norway) for sharing a digital copy of the microdosimetric spectra gathered with respectively the wall-less TEPC, the avalanche-confinement TEPC and the MicroPlus Mushroom at OCL. Anna Bianchi thanks Anna Selva, Valeria Conte and Paolo Colautti (INFN LNL, Italy) for sharing a digital copy of the mini-TEPC microdosimetric spectra.

Author contribution statement

Alessio Parisi conceived the study, performed the computer simulations, analyzed the results and the *in vitro* clonogenic cell survival data. Tatsuhiko Sato provided help with the setup of the simulations and the organization of the study. The experimentally measured microdosimetric spectra were acquired by the authors indicated in the references of Table 1. The RBE values obtained by combining the experimentally measured microdosimetric spectra and the IBWF were calculated by Alessio Parisi (avalanche-confinement TEPC, cylindrical TEPC, diamond detector, Far West LET-1/2 TEPC, MicroPlus Bridge, MicroPlus Mushroom, wall-less TEPC) and Anna Bianchi (mini-TEPC). All authors reviewed and approved the manuscript, written by Alessio Parisi.

References

Aoki, M., Furusawa, Y. and Yamada, T., 2000. LET dependency of heavy-ion induced apoptosis in V79 cells. Journal of radiation research, 41(2), pp.163-175.

Ballarini, F., Altieri, S., Bortolussi, S., Giroletti, E. and Protti, N., 2013. A model of radiation-induced cell killing: insights into mechanisms and applications for hadron therapy. Radiation research, 180(3), pp.307-315.

Belli, M., Cera, F., Cherubini, R., Dalla, M.V., Haque, A.M., Ianzini, F., Moschini, G., Sapora, O., Simone, G., Tabocchini, M.A. and Tiveron, P., 1998. RBE-LET relationships for cell inactivation and mutation induced by low energy protons in V79 cells: further results at the LNL facility. International journal of radiation biology, 74(4), pp.501-509.

Belli, M., Bettega, D., Calzolari, P., Cherubini, R., Cuttone, G., Durante, M., Esposito, G., Furusawa, Y., Gerardi, S., Gialanella, G. and Grossi, G., 2008. Effectiveness of monoenergetic and spread-out bragg peak carbon-ions for inactivation of various normal and tumour human cell lines. Journal of radiation research, 49(6), pp.597-607.

Bird, R.P. and Burki, H.J., 1975. Survival of synchronized Chinese hamster cells exposed to radiation of different linear-energy transfer. International Journal of Radiation Biology and Related Studies in Physics, Chemistry and Medicine, 27(2), pp.105-120.

Blomquist, E., Russell, K.R., Stenerlöw, B., Montelius, A., Grusell, E. and Carlsson, J., 1993. Relative biological effectiveness of intermediate energy protons. Comparisons with 60Co gamma-radiation using two cell lines. Radiotherapy and Oncology, 28(1), pp.44-51.

Bolst, D., Guatelli, S., Tran, L.T., Chartier, L., Lerch, M.L., Matsufuji, N. and Rosenfeld, A.B., 2017. Correction factors to convert microdosimetry measurements in silicon to tissue in 12C ion therapy. Physics in Medicine & Biology, 62(6), p.2055.

Bortot, D., Pola, A., Agosteo, S., Pasquato, S., Mazzucconi, D., Fazzi, A., Colautti, P. and Conte, V., 2017. A novel avalanche-confinement TEPC for microdosimetry at nanometric level. Radiation Measurements, 103, pp.1-12.

Bortot, D., Mazzucconi, D., Pola, A., Fazzi, A., Pullia, M., Savazzi, S., Colautti, P., Conte, V. and Agosteo, S., 2020. A nano-microdosimetric characterization of a therapeutic carbon ion beam at CNAO. Radiation Physics and Chemistry, p.108674.

Böhrnsen, G., Weber, K.J. and Scholz, M., 2002. Measurement of biological effects of high-energy carbon ions at low doses using a semi-automated cell detection system. International journal of radiation biology, 78(4), pp.259-266.

Brenner, D.J. and Zaider, M., 1998. Estimating RBEs at clinical doses from microdosimetric spectra. Medical physics, 25(6), pp.1055-1057.

Britten, R.A., Nazaryan, V., Davis, L.K., Klein, S.B., Nichiporov, D., Mendonca, M.S., Wolanski, M., Nie, X., George, J. and Keppel, C., 2012. Variations in the RBE for cell killing along the depth-dose profile of a modulated proton therapy beam. Radiation research, 179(1), pp.21-28.

Carante, M.P., Aimè, C., Cajiao, J.J.T. and Ballarini, F., 2018. BIANCA, a biophysical model of cell survival and chromosome damage by protons, C-ions and He-ions at energies and doses used in hadrontherapy. Physics in Medicine & Biology, 63(7), p.075007.

Carlson, D.J., Stewart, R.D., Semenenko, V.A. and Sandison, G.A., 2008. Combined use of Monte Carlo DNA damage simulations and deterministic repair models to examine putative mechanisms of cell killing. Radiation research, 169(4), pp.447-459.

Caswell, R.S. and Coyne, J.J., 1989. Effects of track structure on neutron microdosimetry and nanodosimetry. International Journal of Radiation Applications and Instrumentation. Part D. Nuclear Tracks and Radiation Measurements, 16(2-3), pp.187-195.

Chaudhary, P., Marshall, T.I., Perozziello, F.M., Manti, L., Currell, F.J., Hanton, F., McMahon, S.J., Kavanagh, J.N., Cirrone, G.A.P., Romano, F. and Prise, K.M., 2014. Relative biological effectiveness variation along monoenergetic and modulated Bragg peaks of a 62-MeV therapeutic proton beam: a preclinical assessment. International Journal of Radiation Oncology* Biology* Physics, 90(1), pp.27-35.

Chen, Y., Li, J., Li, C., Qiu, R. and Wu, Z., 2017. A modified microdosimetric kinetic model for relative biological effectiveness calculation. Physics in Medicine & Biology, 63(1), p.015008.

Colautti, P., Conte, V., Selva, A., Chiriotti, S., Pola, A., Bortot, D., Fazzi, A., Agosteo, S., Treccani, M., De Nardo, L. and Verona, C., 2018. Miniaturized microdosimeters as LET monitors: First comparison of calculated and experimental data performed at the 62 MeV/u 12C beam of INFN-LNS with four different detectors. Physica Medica, 52, pp.113-121.

Colautti, P., Bianchi, A., Selva, A., Bortot, D., Mazzucconi, D., Pola, A., Agosteo, S., Petringa, G., Cirrone, G.A.P. and Conte, V., 2020. Therapeutic proton beams: LET, RBE and microdosimetric spectra with gas and silicon detectors. Radiation Measurements, p.106386.

Conte, V., Colautti, P., Chiriotti, S., Moros, D., Ciocca, M. and Mairani, A., 2017. Mini-TEPC Microdosimetric Study of Carbon Ion Therapeutic Beams at CNAO. In EPJ Web of Conferences (Vol. 153, p. 01012). EDP Sciences.

Conte, V., Bianchi, A., Selva, A., Petringa, G., Cirrone, G.A.P., Parisi, A., Vanhavere, F. and Colautti, P., 2019. Microdosimetry at the CATANA 62 MeV proton beam with a sealed miniaturized TEPC. Physica Medica, 64, pp.114-122.

Cox, R., Thacker, J., Goodhead, D.T. and Munson, R.J., 1977 a. Mutation and inactivation of mammalian cells by various ionising radiations. Nature, 267, pp.425-427.

Cox, R., Thacker, J., Goodhead, D.T., Masson, W.K. and Wilkinson, R.E., 1977 b. Inactivation and mutation of cultured mammalian cells by aluminium characteristic ultrasoft x-rays: II. Dose-responses of Chinese hamster

and human diploid cells to aluminium x-rays and radiations of different LET. International Journal of Radiation Biology and Related Studies in Physics, Chemistry and Medicine, 31(6), pp.561-576.

Cunha, Micaela, Caterina Monini, Etienne Testa, and Michael Beuve. "NanOx, a new model to predict cell survival in the context of particle therapy." Physics in Medicine & Biology 62, no. 4 (2017): 1248.

De Nardo, L., Cesari, V., Donà, G., Magrin, G., Colautti, P., Conte, V. and Tornielli, G., 2004 a. Mini-TEPCs for radiation therapy. Radiation protection dosimetry, 108(4), pp.345-352.

De Nardo, L., Cesari, V., Iborra, N., Conte, V., Colautti, P., Hérault, J., ., Tornielli, G. and Chauvel, P, 2004 b. Microdosimetric Assessment of Nice Therapeutic Proton Beam Biological Quality. Microdosimetric Assessment of Nice Therapeutic Proton Beam Biological Quality. Physica Medica, XX, 2, pp. 71-77.

Doria, D., Kakolee, K.F., Kar, S., Litt, S.K., Fiorini, F., Ahmed, H., Green, S., Jeynes, J.C.G., Kavanagh, J., Kirby, D. and Kirkby, K.J., 2012. Biological effectiveness on live cells of laser driven protons at dose rates exceeding 109 Gy/s. AIP Advances, 2(1), p.011209.

Durante, M. and Paganetti, H., 2016. Nuclear physics in particle therapy: a review. Reports on Progress in Physics, 79(9), p.096702.

Elsässer, T. and Scholz, M., 2007. Cluster effects within the local effect model. Radiation research, 167(3), pp.319-329.

Elsässer, T., Weyrather, W.K., Friedrich, T., Durante, M., Iancu, G., Krämer, M., Kragl, G., Brons, S., Winter, M., Weber, K.J. and Scholz, M., 2010. Quantification of the relative biological effectiveness for ion beam radiotherapy: direct experimental comparison of proton and carbon ion beams and a novel approach for treatment planning. International Journal of Radiation Oncology* Biology* Physics, 78(4), pp.1177-1183.

Folkard, M., Prise, K.M., Vojnovic, B., Davies, S., Roper, M.J. and Michael, B.D., 1989. The irradiation of V79 mammalian cells by protons with energies below 2 MeV: part I: experimental arrangement and measurements of cell survival. International journal of radiation biology, 56(3), pp.221-237.

Folkard, M., 1996. Inactivation of V79 cells by low-energy protons, deuterons and helium-3 ions. International journal of radiation biology, 69(6), pp.729-738.

Frese, M.C., Victor, K.Y., Stewart, R.D. and Carlson, D.J., 2012. A mechanism-based approach to predict the relative biological effectiveness of protons and carbon ions in radiation therapy. International Journal of Radiation Oncology* Biology* Physics, 83(1), pp.442-450.

Friedland, W., Schmitt, E., Kundrat, P., Dingfelder, M., Baiocco, G., Barbieri, S. and Ottolenghi, A., 2017. Comprehensive track-structure based evaluation of DNA damage by light ions from radiotherapy-relevant energies down to stopping. Scientific reports, 7(1), pp.1-15.

Friedrich, T., Durante, M. and Scholz, M., 2012. Modeling cell survival after photon irradiation based on double-strand break clustering in megabase pair chromatin loops. Radiation research, 178(5), pp.385-394.

Friedrich, T., Scholz, U., Elsässer, T., Durante, M. and Scholz, M., 2013. Systematic analysis of RBE and related quantities using a database of cell survival experiments with ion beam irradiation. Journal of radiation research, 54(3), pp.494-514.

Friedrich, T., Durante, M. and Scholz, M., 2014. Modeling cell survival after irradiation with ultrasoft X rays using the giant loop binary lesion model. Radiation Research, 181(5), pp.485-494.

Furusawa, Y., Fukutsu, K., Aoki, M., Itsukaichi, H., Eguchi-Kasai, K., Ohara, H., Yatagai, F., Kanai, T. and Ando, K., 2000. Inactivation of aerobic and hypoxic cells from three different cell lines by accelerated 3He-, 12C-and 20Ne-ion beams. Radiation research, 154(5), pp.485-496.

Furusawa, Y., Aoki, M. and Durante, M., 2002. Simultaneous exposure of mammalian cells to heavy ions and X-rays. Advances in Space Research, 30(4), pp.877-884.

Gerelchuluun, A., Manabe, E., Ishikawa, T., Sun, L., Itoh, K., Sakae, T., Suzuki, K., Hirayama, R., Asaithamby, A., Chen, D.J. and Tsuboi, K., 2015. The major DNA repair pathway after both proton and carbon-ion radiation is NHEJ, but the HR pathway is more relevant in carbon ions. Radiation research, 183(3), pp.345-356.

Gerlach, R., Roos, H. and M. Kellerer, A., 2002. Heavy ion RBE and microdosimetric spectra. Radiation protection dosimetry, 99(1-4), pp.413-418.

Guan, F., Geng, C., Carlson, D.J., Ma, D.H., Bronk, L., Gates, D., Wang, X., Kry, S.F., Grosshans, D. and Mohan, R., 2018. A mechanistic relative biological effectiveness model-based biological dose optimization for charged particle radiobiology studies. Physics in Medicine & Biology, 64(1), p.015008.

Hall, E.J., Gross, W., Dvorak, R.F., Kellerer, A.M. and Rossi, H.H., 1972. Survival curves and age response functions for Chinese hamster cells exposed to X-rays or high LET alpha-particles. Radiation research, 52(1), pp.88-98.

Hall, E.J., Bird, R.P., Rossi, H.H., Coffey, R., Varga, J. and Lam, Y.M., 1977. Biophysical studies with high-energy argon ions 2. Determinations of the relative biological effectiveness, the oxygen enhancement ratio, and the cell cycle response. Radiation research, 70(3), pp.469-479.

Hawkins, R.B., 1994. A statistical theory of cell killing by radiation of varying linear energy transfer. Radiation research, 140(3), pp.366-374.

Hawkins, R.B., 2003. A microdosimetric-kinetic model for the effect of non-Poisson distribution of lethal lesions on the variation of RBE with LET. Radiation research, 160(1), pp.61-69.

Hu, N., Tanaka, H., Takata, T., Endo, S., Masunaga, S., Suzuki, M. and Sakurai, Y., 2020. Evaluation of PHITS for microdosimetry in BNCT to support radiobiological research. Applied Radiation and Isotopes, p.109148.

Hirayama, R., Ito, A., Tomita, M., Tsukada, T., Yatagai, F., Noguchi, M., Matsumoto, Y., Kase, Y., Ando, K., Okayasu, R. and Furusawa, Y., 2009. Contributions of direct and indirect actions in cell killing by high-LET radiations. Radiation research, 171(2), pp.212-218.

Inaniwa, T. and Kanematsu, N., 2018. Adaptation of stochastic microdosimetric kinetic model for charged-particle therapy treatment planning. Physics in Medicine & Biology, 63(9), p.095011.

International Commission on Radiation Units and Measurements, 1983. ICRU Report 36 Microdosimetry. Bethesda, International Commission on Radiation Units and Measurements.

Jenner, T.J., Delara, C.M., O'Neill, P.S.D.L. and Stevens, D.L., 1993. Induction and rejoining of DNA double-strand breaks in V79-4 mammalian cells following γ-and α-irradiation. International journal of radiation biology, 64(3), pp.265-273.

Jeynes, J.C.G., Merchant, M.J., Barazzuol, L., Barry, M., Guest, D., Palitsin, V.V., Grime, G.W., Tullis, I.D.C., Barber, P.R., Vojnovic, B. and Kirkby, K.J., 2013. "Broadbeam" irradiation of mammalian cells using a vertical microbeam facility. Radiation and environmental biophysics, 52(4), pp.513-521.

Kase, Y., Kanai, T., Matsumoto, Y., Furusawa, Y., Okamoto, H., Asaba, T., Sakama, M. and Shinoda, H., 2006. Microdosimetric measurements and estimation of human cell survival for heavy-ion beams. Radiation research, 166(4), pp.629-638.

Kase, Y., Himukai, T., Nagano, A., Tameshige, Y., Minohara, S., Matsufuji, N., Mizoe, J., Fossati, P., Hasegawa, A. and Kanai, T., 2011. Preliminary calculation of RBE-weighted dose distribution for cerebral radionecrosis in carbon-ion treatment planning. Journal of radiation research, pp.1109140229-1109140229.

Kase, Y., Yamashita, W., Matsufuji, N., Takada, K., Sakae, T., Furusawa, Y., Yamashita, H. and Murayama, S., 2012. Microdosimetric calculation of relative biological effectiveness for design of therapeutic proton beams. Journal of radiation research, 54(3), pp.485-493.

Katz, R., Ackerson, B., Homayoonfar, M. and Sharma, S.C., 1971. Inactivation of cells by heavy ion bombardment. Radiation research, 47(2), pp.402-425.

Katz, R., 1978. Track structure theory in radiobiology and in radiation detection. Nuclear track detection, 2(1), pp.1-28.

Kellerer, A.M. and Rossi, H.H., 1974. The theory of dual radiation action. Current Topics in Radiation Research Quarterly, pp.85-158.

Kellerer, A.M. and Rossi, H.H., 1978. A generalized formulation of dual radiation action. Radiation research, 75(3), pp.471-488.

Loncol, T., Cosgrove, V., Denis, J.M., Gueulette, J., Mazal, A., Menzel, H.G., Pihet, P. and Sabattier, R., 1994. Radiobiological effectiveness of radiation beams with broad LET spectra: microdosimetric analysis using biological weighting functions. Radiation Protection Dosimetry, 52(1-4), pp.347-352.

Magrin, G., 2018. A method to convert spectra from slab microdosimeters in therapeutic ion-beams to the spectra referring to microdosimeters of different shapes and material. Physics in Medicine & Biology, 63(21), p.215021.

Magrin, G., Verona, C., Ciocca, M., Marinelli, M., Mastella, E., Stock, M. and Verona-Rinati, G., 2019. Microdosimetric characterization of clinical carbon-ion beams using synthetic diamond detectors and spectral conversion methods. Medical physics.

Matsuya, Y., Sasaki, K., Yoshii, Y., Okuyama, G. and Date, H., 2018. Integrated modelling of cell responses after irradiation for DNA-targeted effects and non-targeted effects. Scientific reports, 8(1), pp.1-14.

Mazzucconi, D., Bortot, D., Pola, A., Fazzi, A., Colautti, P., Conte, V., Petringa, G., Cirrone, G.A.P. and Agosteo, S., 2019. Nano-microdosimetric investigation at the therapeutic proton irradiation line of CATANA. Radiation Measurements, 123, pp.26-33.

McMahon, S.J., Schuemann, J., Paganetti, H. and Prise, K.M., 2016. Mechanistic modelling of DNA repair and cellular survival following radiation-induced DNA damage. Scientific reports, 6(1), pp.1-14.

McMahon, S.J., McNamara, A.L., Schuemann, J., Paganetti, H. and Prise, K.M., 2017. A general mechanistic model enables predictions of the biological effectiveness of different qualities of radiation. Scientific reports, 7(1), p.10790.

McMahon, S.J., 2018. The linear quadratic model: usage, interpretation and challenges. Physics in Medicine & Biology, 64(1), p.01TR01.

McMahon, S.J. and Prise, K.M., 2019. Mechanistic modelling of radiation responses. Cancers, 11(2), p.205.

Monini, C., Cunha, M., Testa, E. and Beuve, M., 2018. Study of the Influence of NanOx Parameters. Cancers, 10(4), p.87.

Morstin, K., Bond, V.P. and Baum, J.W., 1989. Probabilistic approach to obtain hit-size effectiveness functions which relate microdosimetry and radiobiology. Radiation research, 120(3), pp.383-402.

Olko, P., Bilski, P., Budzanowski, M., Waligórski, M.P.R. and Reitz, G., 2002. Modeling the response of thermoluminescence detectors exposed to low-and high-LET radiation fields. Journal of radiation research, 43(S), pp.S59-S62.

Paganetti, H., Olko, P., Kobus, H., Becker, R., Schmitz, T., Waligorski, M.P., Filges, D. and Müller-Gärtner, H.W., 1997. Calculation of relative biological effectiveness for proton beams using biological weighting functions. International Journal of Radiation Oncology* Biology* Physics, 37(3), pp.719-729.

Paganetti, H., 2014. Relative biological effectiveness (RBE) values for proton beam therapy. Variations as a function of biological endpoint, dose, and linear energy transfer. Physics in Medicine & Biology, 59(22), p.R419.

Paganetti, H., Blakely, E., Carabe-Fernandez, A., Carlson, D.J., Das, I.J., Dong, L., Grosshans, D., Held, K.D., Mohan, R., Moiseenko, V. and Niemierko, A., 2019. Report of the AAPM TG-256 on the relative biological effectiveness of proton beams in radiation therapy. Medical physics, 46(3), pp.e53-e78.

Parisi, A., Van Hoey, O., Mégret, P. and Vanhavere, F., 2019. Microdosimetric specific energy probability distribution in nanometric targets and its correlation with the efficiency of thermoluminescent detectors exposed to charged particles. Radiation Measurements, 123, pp.1-12.

Perris, A., Pialoglou, P., Katsanos, A.A. and Sideris, E.G., 1986. Biological effectiveness of low energy protons. I. Survival of Chinese hamster cells. International Journal of Radiation Biology and Related Studies in Physics, Chemistry and Medicine, 50(6), pp.1093-1101.

Pihet, P., Menzel, H.G., Schmidt, R., Beauduin, M. and Wambersie, A., 1990. Biological weighting function for RBE specification of neutron therapy beams. Intercomparison of 9 European centres. Radiation Protection Dosimetry, 31(1-4), pp.437-442.

Pihet, P. and Menzel, H.G., 1999. Response to the Letter to the Editor "Estimating RBEs at clinical doses from microdosimetric spectra"[Med. Phys. 25, 1055 (1998)]. Medical physics, 26(5), pp.848-852.

Prise, K.M., Folkard, M., Davies, S. and Michael, B.D., 1990. The irradiation of V79 mammalian cells by protons with energies below 2 MeV. Part II. Measurement of oxygen enhancement ratios and DNA damage. International journal of radiation biology, 58(2), pp.261-277.

Raju, M.R., Eisen, Y., Carpenter, S. and Inkret, W.C., 1991. Radiobiology of α particles: III. Cell inactivation by α-particle traversals of the cell nucleus. Radiation research, 128(2), pp.204-209.

Samnøy, A.T., Ytre-Hauge, K.S., Malinen, E., Tran, L., Rosenfeld, A., Povoli, M., Kok, A., Summanwar, A. and Röhrich, D., 2020. Microdosimetry with a 3D silicon on insulator (SOI) detector in a low energy proton beamline. Radiation Physics and Chemistry, p.109078.

Sato, T., Watanabe, R. and Niita, K., 2006. Development of a calculation method for estimating specific energy distribution in complex radiation fields. Radiation protection dosimetry, 122(1-4), pp.41-45.

Sato, T. and Furusawa, Y., 2012. Cell survival fraction estimation based on the probability densities of domain and cell nucleus specific energies using improved microdosimetric kinetic models. Radiation research, 178(4), pp.341-356.

Sato, T., Watanabe, R., Sihver, L. and Niita, K., 2012. Applications of the microdosimetric function implemented in the macroscopic particle transport simulation code PHITS. International journal of radiation biology, 88(1-2), pp.143-150.

Sato, T. and Hamada, N., 2014. Model assembly for estimating cell surviving fraction for both targeted and nontargeted effects based on microdosimetric probability densities. PloS one, 9(11), p.e114056.

Sato, T., Iwamoto, Y., Hashimoto, S., Ogawa, T., Furuta, T., Abe, S.I., Kai, T., Tsai, P.E., Matsuda, N., Iwase, H. and Shigyo, N., 2018. Features of particle and heavy ion transport code system (PHITS) version 3.02. Journal of Nuclear Science and Technology, 55(6), pp.684-690.

Schmollack, J.U., Klaumuenzer, S.L. and Kiefer, J., 2000. Stochastic radial dose distributions and track structure theory. Radiation research, 153(4), pp.469-478.

Scholz, M., Kellerer, A.M., Kraft-Weyrather, W. and Kraft, G., 1997. Computation of cell survival in heavy ion beams for therapy. Radiation and environmental biophysics, 36(1), pp.59-66.

Scholz, M., 2003. Effects of ion radiation on cells and tissues. In Radiation effects on polymers for biological use (pp. 95-155). Springer, Berlin, Heidelberg.

Schuff, J.A., Policastro, L., Duran, H., Kreiner, A.J., Mazal, A., Molinari, B.L., Burlon, A., Debray, M.E., Kesque, J.M., Somacal, H. and Stoliar, P., 2002. Relative biological effectiveness measurements of low energy proton and lithium beams on tumor cells. Nuclear Instruments and Methods in Physics Research Section B: Beam Interactions with Materials and Atoms, 187(3), pp.345-353.

Stenerlöw, B., Pettersson, O.A., Essand, M., Blomquist, E. and Carlsson, J., 1995. Irregular variations in radiation sensitivity when the linear energy transfer is increased. Radiotherapy and Oncology, 36(2), pp.133-142.

Takada, K., Sato, T., Kumada, H., Koketsu, J., Takei, H., Sakurai, H. and Sakae, T., 2018. Validation of the physical and RBE-weighted dose estimator based on PHITS coupled with a microdosimetric kinetic model for proton therapy. Journal of radiation research, 59(1), pp.91-99.

Thacker, J., Stretch, A. and Stephens, M.A., 1979. Mutation and inactivation of cultured mammalian cells exposed to beams of accelerated heavy ions: II. Chinese hamster V79 cells. International Journal of Radiation Biology and Related Studies in Physics, Chemistry and Medicine, 36(2), pp.137-148.

Tilly, N., 1999. Comparison of cell survival models for mixed LET radiation. International journal of radiation biology, 75(2), pp.233-243.

Tomita, H., Kai, M., Kusama, T. and Ito, A., 1997. Monte Carlo simulation of physicochemical processes of liquid water radiolysis. Radiation and environmental biophysics, 36(2), pp.105-116.

Tran, L.T., Chartier, L., Bolst, D., Prokopovich, D.A., Guatelli, S., Nancarrow, M., Reinhard, M.I., Petasecca, M., Lerch, M.L., Pereverlaylo, V.L. and Matsufuji, N., 2015. 3D Silicon Microdosimetry and RBE Study Using 12C Ion of Different Energies. IEEE Transactions on Nuclear Science, 62(6), pp.3027-3033.

Tran, L.T., Chartier, L., Bolst, D., Pogossov, A., Guatelli, S., Petasecca, M., Lerch, M.L., Prokopovich, D.A., Reinhard, M.I., Clasie, B., Depauw, N., Kooy, H., Flanz, J. B., McNamara, A., Paganetti, H., Beltran, H., Furutani, K., Perevertaylo, V. L., Jackson, M. and Rosenfeld, A. B., 2017 a. Characterization of proton pencil beam scanning and passive beam using a high spatial resolution solid-state microdosimeter. Medical physics, 44(11), pp.6085-6095.

Tran, L.T., Chartier, L., Prokopovich, D.A., Bolst, D., Povoli, M., Summanwar, A., Kok, A., Pogossov, A., Petasecca, M., Guatelli, S. and Reinhard, M.I., 2017 b. Thin silicon microdosimeter utilizing 3-D MEMS fabrication technology: Charge collection study and its application in mixed radiation fields. IEEE Transactions on Nuclear Science, 65(1), pp.467-472.

Tran, L.T., Chartier, L., Bolst, D., Davis, J., Prokopovich, D.A., Pogossov, A., Guatelli, S., Reinhard, M.I., Petasecca, M., Lerch, M.L. and Matsufuji, N., 2018. In-field and out-of-file application in 12C ion therapy using fully 3D silicon microdosimeters. Radiation Measurements, 115, pp.55-59.

Tsuda, S., Sato, T., Takahashi, F., Satoh, D., Endo, A., Sasaki, S., Namito, Y., Iwase, H., Ban, S. and Takada, M., 2010. Measurement of microdosimetric spectra with a wall-less tissue-equivalent proportional counter for a 290 MeV/u 12C beam. Physics in Medicine & Biology, 55(17), p.5089.

Tsuda, S., Sato, T., Takahashi, F., Satoh, D., Sasaki, S., Namito, Y., Iwase, H., Ban, S. and Takada, M., 2012. Systematic measurement of lineal energy distributions for proton, He and Si ion beams over a wide energy range using a wall-less tissue equivalent proportional counter. Journal of radiation research, 53(2), pp.264-271.

Verona, C., Magrin, G., Solevi, P., Grilj, V., Jakšić, M., Mayer, R., Marinelli, M. and Verona-Rinati, G., 2015. Spectroscopic properties and radiation damage investigation of a diamond based Schottky diode for ion-beam therapy microdosimetry. Journal of Applied Physics, 118(18), p.184503.

Weber, K.J. and Flentje, M., 1993. Lethality of heavy ion-induced DNA double-strand breaks in mammalian cells. International journal of radiation biology, 64(2), pp.169-178.

Weyrather, W.K., Ritter, S., Scholz, M. and Kraft, G., 1999. RBE for carbon track-segment irradiation in cell lines of differing repair capacity. International journal of radiation biology, 75(11), p.1357.

Wouters, B.G., Lam, G.K.Y., Oelfke, U., Gardey, K., Durand, R.E. and Skarsgard, L.D., 1996. Measurements of relative biological effectiveness of the 70 MeV proton beam at TRIUMF using Chinese hamster V79 cells and the high-precision cell sorter assay. Radiation research, 146(2), pp.159-170.

Wouters, B.G., Skarsgard, L.D., Gerweck, L.E., Carabe-Fernandez, A., Wong, M., Durand, R.E., Nielson, D., Bussiere, M.R., Wagner, M., Biggs, P. and Paganetti, H., 2015. Radiobiological intercomparison of the 160 MeV and 230 MeV proton therapy beams at the Harvard Cyclotron Laboratory and at Massachusetts General Hospital. Radiation research, 183(2), pp.174-187.

Wroe, A., Schulte, R., Fazzi, A., Pola, A., Agosteo, S. and Rosenfeld, A., 2009. RBE estimation of proton radiation fields using a telescope. Medical physics, 36(10), pp.4486-4494.

Wulf, H., Kraft-Weyrather, W., Miltenburger, H.G., Blakely, E.A., Tobias, C.A. and Kraft, G., 1985. Heavy-ion effects on mammalian cells: inactivation measurements with different cell lines. Radiation Research, 104(2s), pp.S122-S134.

Zhou, G., Kawata, T., Furusawa, Y., Aoki, M., Hirayama, R., Ando, K. and Ito, H., 2006. Protective effects of melatonin against low-and high-LET irradiation. Journal of radiation research, 47(2), pp.175-181.

Zhu, H., Chen, Y., Sung, W., McNamara, A.L., Tran, L.T., Burigo, L.N., Rosenfeld, A.B., Li, J., Faddegon, B., Schuemann, J. and Paganetti, H., 2019. The microdosimetric extension in TOPAS: development and comparison with published data. Physics in Medicine & Biology, 64(14), p.145004.

Ziegler, J.F., Ziegler, M.D. and Biersack, J.P., 2010. SRIM–The stopping and range of ions in matter (2010). Nuclear Instruments and Methods in Physics Research Section B: Beam Interactions with Materials and Atoms, 268(11-12), pp.1818-1823.